UNIVERSITY OF MANITOBA

Numerical Simulation of Transient Liquid Phase Bonding with Variable Diffusion Coefficient in Planar, Cylindrical and Spherical Systems

By

Amin Ghanbar

A thesis submitted to

The Faculty of Graduate Studies

In partial fulfillment of the requirement for the degree of

MASTER OF SCIENCE

Department of Mechanical and Manufacturing Engineering

University of Manitoba

Winnipeg, Manitoba

January 2019

Abstract

A new finite difference numerical model with variable diffusion coefficient is developed by using an explicit-fully-implicit hybrid method and Landau transformation with adaptable spatial discretization to study TLP bonding kinetics in planar and non-planar systems. The results of the numerical model developed in this research, which are verified with experimental data available in the literature, reveal key reasons for why the extent of isothermal solidification deviates from linear relationship with $\sqrt{t}$, i.e. deviation from parabolic behavior. The deviation occurs when the concentration dependency of D changes with time. In non-planar systems (cylindrical and spherical), however, deviation from the parabolic behavior can occur even when D is independent of both concentration and time, solely by geometry-induced effect. Moreover, the kinetics of solute penetration into the substrate during isothermal solidification is different from the solute penetration kinetics that occur during homogenization process that follows the isothermal solidification stage.

Acknowledgments

Firstly, I would like to express my sincere gratitude to my advisor, Dr. O. A. Ojo, for his encouragements, guidance, patience, and support. This project would not have been possible without his assistance. Secondly, I would like to thank my parents and my brother for supporting me over the years. Finally, I am grateful to Sydney Van Aert, Mallikarjuna Heggadadevanapura Thammaiah, Nnaemeka Ugodilinwa, and Mohammad Reza Kazemian, for their companionship during this journey and assistance with various aspects of the research.

List of Abbreviations and Symbols

TLP: **T**ransient **L**iquid **P**hase

MPD: **M**elting **P**oint **D**epressant

D: **D**iffusion coefficient

IS: **I**sothermal **S**olidification

C: Concentration

x: Distance

L: Total width of base metal and half width of interlayer

t: Time

$D_{(c)}$: Concentration-dependent diffusion coefficient

$D_{(c,t)}$: Concentration and time-dependent diffusion coefficient

$\emptyset$: Isothermal solidification rate constant

K: Constant value

Y: Isothermal solidification width

$C_{\alpha L}$: Equilibrium solute concentration in the solid phase next to the interlayer

$C_{L\alpha}$: Equilibrium solute concentration in the Liquid phase next to the interlayer

s: Interface position

W_{max}: Maximum dissolution width

W_0: Initial thickness of the filler alloy

t_f: The time required to complete isothermal solidification

h: Width of the interlayer metal

C_0: Initial solute concentration in the interlayer

C_M: Initial solute concentration in the base metal

i: Node number of distance

j: Node number of time

a: Local position in the liquid phase

b: Local position in the solid phase

m: Exponent

g: Geometry factor

H_p: Depth of solute penetration during homogenization

IS_p: Depth of solute penetration during isothermal solidification

r: Radius

R_D: Ratio of diffusion coefficient

R_K: Ratio of constant value K

G_{dev}: Extent of geometry-induce deviation

r_0: Initial radius of solid-liquid interface curvature

Table of Contents

List of Figures

Chapter 1. Introduction

1.1. Background

Transient liquid phase (TLP) bonding is an effective technique for joining advance materials such as aerospace nickel-based superalloys that are extremely susceptible to cracking during conventional welding methods. However, one of the significant problems of TLP bonding is that the time required to complete the joining process is significantly high [1]. On the other hand, insufficient holding time can result in the formation of deleterious micro-constituents within the joint region, which can degrade mechanical and corrosion properties [2].

Many researchers have reported that TLP bonding processing time can be affected by parameters such as temperature, the initial thickness of filler and base metals, the diffusion coefficient of melting point depressant (MPD) elements, and interlayer chemical compositions [1][3][4]. Hence, a proper selection of these parameters can minimize the total time required to complete the TLP bonding process, which can translate to significant cost reduction due to a decrease in labor and repair time. Studying the effect of these parameters on the TLP bonding process through experiments is not economical. Therefore, numerous models have been developed and used to understand the TLP bonding kinetics. However, these TLP bonding models assume constant diffusion coefficients in a planar system to simplify calculations [5][6][7][8][9]. Hence, a more reliable model is required to investigate the effect of variable diffusion coefficients on the kinetics of TLP bonding.

1.2. Objective

The goal of the present work is to develop a new numerical TLP bonding model that incorporates variable diffusion coefficient, instead of the commonly assumed constant diffusivity, and use the model to systematically study the kinetics of isothermal solidification and homogenization in planar, cylindrical, and spherical systems.

1.3. Work Done

A new numerical model by finite difference method, in which an explicit-fully-implicit hybrid approach combined with Landau transformation that utilizes adaptable spatial discretization, to calculate and analyse diffusion controlled solid-liquid interface migration during the TLP bonding process is developed. The new model, which enables the use of variable diffusion coefficient, is applied to study isothermal solidification and homogenization kinetics in planar, cylindrical, and spherical systems. Major results of the new model are successfully verified by using previously reported experimental data.

1.4. Major Findings

A new numerical model capable of analyzing the TLP bonding process with variable D is developed and used to carefully study the effect of variable diffusivity on the isothermal solidification and homogenization kinetics in planar, cylindrical, and spherical systems. The results show that when D varies with concentration, ($D_{(C)}$), the kinetics of isothermal solidification stage of the process can be significantly affected. In a planar system, when D is solely dependent on concentration, a linear relationship exists between the diffusion-controlled solid-liquid interface migration and $\sqrt{t}$. In such a situation, the kinetics of the process can be

represented by a constant parameter, $\emptyset$, known as isothermal solidification rate constant and it is given by the slope of the linear relationship plot. At a constant temperature, when the function that determines the dependency of D on concentration, $F(D_{(c)})$, varies with time, $\emptyset$ ceases to be a constant parameter, as deviation from the parabolic relationship between the solid-liquid interface migration and holding time occurs. This finding, which is validated by reported experimental data, provides a new explanation for the deviation occurrence that could not be explicated by prior suggested concepts. Furthermore, in cases where $F(D_{(c)})$ does not change with temperature, increase in temperature generally produces an isothermally constant $\emptyset$ that increases with temperature. However, when $F(D_{(c)})$ varies with temperature, it is possible for the isothermally constant $\emptyset$ to decrease with increase in temperature, a situation that is not commonly reported in the literature.

In contrast to the planar system, the kinetics of isothermal solidification in cylindrical and spherical systems cannot be represented by a constant parameter $\emptyset$, even when D is constant and independent on both concentration and time. This type of deviation behavior, which is fundamentally geometry-induced, can produce a situation that never occurs in the planar system, where the size of the substrate material can influence the isothermal solidification kinetics, even when the diffusion solute does reach the center of the base-material. Furthermore, it is found that the kinetics of diffusion-controlled solute penetration into the substrate material during the homogenization stage that follows complete isothermal solidification are significantly different from those that occur during the isothermal solidification process. During homogenization, a parabolic relationship exists between the extent of solute penetration and holding time, when D is constant in planar, cylindrical and spherical systems. This is at variance to what occurs during isothermal solidification, where deviation from the parabolic relationship between solute

penetration and time occurs when D is constant in cylindrical and spherical systems. Moreover, although the solute penetration depth increases linearly with $\sqrt{t}$, when D varies with concentration in a planar system during isothermal solidification, under a similar condition, there is a deviation from the linear relationship during the homogenization process.

1.5. Thesis Layout

This thesis contains six chapters, organized as follows:

- Chapter 1 provides background information, the objective of the present study, work done, and major findings.
- Chapter 2 provides a literature survey focusing on mechanisms of the TLP bonding process, salient parameters, and previous TLP bonding numerical and analytical models.
- Chapter 3 discusses the development and validation of a new finite difference numerical model with variable diffusion coefficient in planar, cylindrical, and spherical systems.
- Chapter 4 contains the presentation and discussion of numerical simulation results of the influence of variable diffussivity on the kinetics of the isothermal solidification and homogenization stages of TLP bonding in planar, cylindrical, and spherical systems.
- Chapter 5 contains a summary and conclusions.
- Chapter 6 provides suggestions for future work.

Chapter 2: Literature Review

2.1. Mechanism of the Transient Liquid Phase (TLP) Bonding

2.1.1. Background

Transient liquid phase (TLP) bonding is a joining technique for several types of heat resistant and difficult-to-weld materials in aerospace applications, such as nickel-based superalloys [10]. During this process, an interlayer material, also known as a filler alloy and used for the bonding process, contains melting point depressant (MPD) element(s), for instance, phosphorous (P), silicon (Si) and boron (B). The MPD elements that are normally selected for bonding applications are those that usually diffuse fast in the solid substrate during joining [11]. At the bonding temperature, the filler metal melts between two base metals. Due to the diffusion of the MPD element(s) from the filler alloy into the solid, the region of the base metals next to the solid-liquid interlayer melts, which results in increasing the volume of the liquid phase. After the melting process, further solid-state diffusion of MPD elements into the solid phase at a constant bonding temperature makes the solid-liquid interface migrate toward the liquid phase until the liquid phase is fully solidified. This type of solidification at a constant temperature, which is known as isothermal solidification, is driven by the slow rate of solid-state diffusion. Hence, the extended holding time is required to complete isothermal solidification. After that, the bonded metals may be held at an elevated temperature for an extended period to homogenize the compositions.

The TLP bonding process has been defined by Duvall et al. [2] as three stages as i) Base metal dissolution; ii) Isothermal solidification; and, iii) Homogenization. However, it was observed that during the heating process, some solid-state diffusion of MPD element(s) can take place. This diffusion occurrence depends on heating rate, the diffusivity of MPD element(s) and the bonding temperature. Hence, due to the loss of solute during the heating process, this stage has been considered to be one of the stages of TLP bonding [12]. Therefore, as it is illustrated in Figure 1, Zhou et al. [13] and Tuah-Poku [14] reclassified four stages for the TLP bonding process as follows:

Stage 1: Heating

Stage 2: Dissolution

Stage 3: Isothermal solidification

Stage 4: Homogenization

Figures 1 and 2 can be used to describe the stages of the TLP bonding process and the fundamental mechanisms of this process. As it is shown in Figure 1, the interlayer with an initial thickness of filler metal (W_0) contains an initial MPD concentration of C_F. During the dissolution and isothermal solidification processes, boundary conditions are as follows:

$$\begin{cases} C = C_{L\alpha}, & x = s^+ \\ C = C_{\alpha L}, & x = s^- \end{cases}, \quad t > 0 \qquad \text{Equation 1}$$

Where $C_{L\alpha}$ and $C_{\alpha L}$ are the equilibrium solute concentrations in the liquid and solid phases next to the interlayer respectively, s is the position of the interface, and t is the processing time.

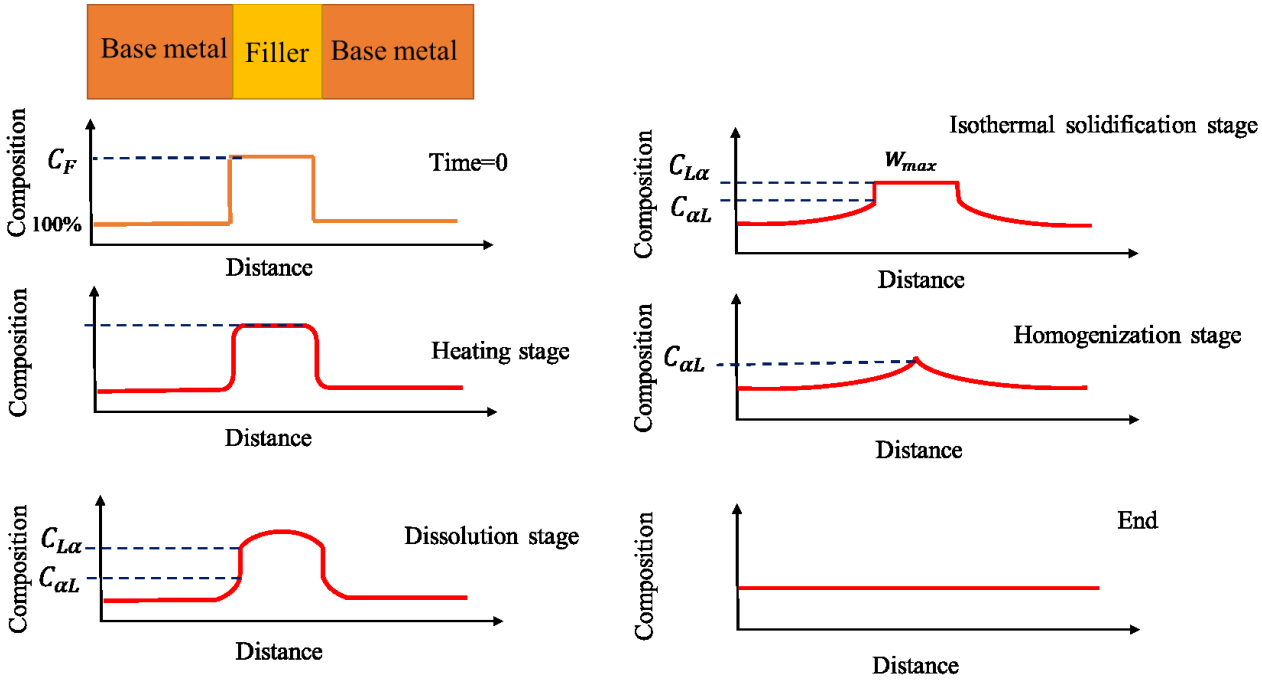

Figure 1: Schematic illustration of all TLP bonding stages as defined by Zhou et al. [13].

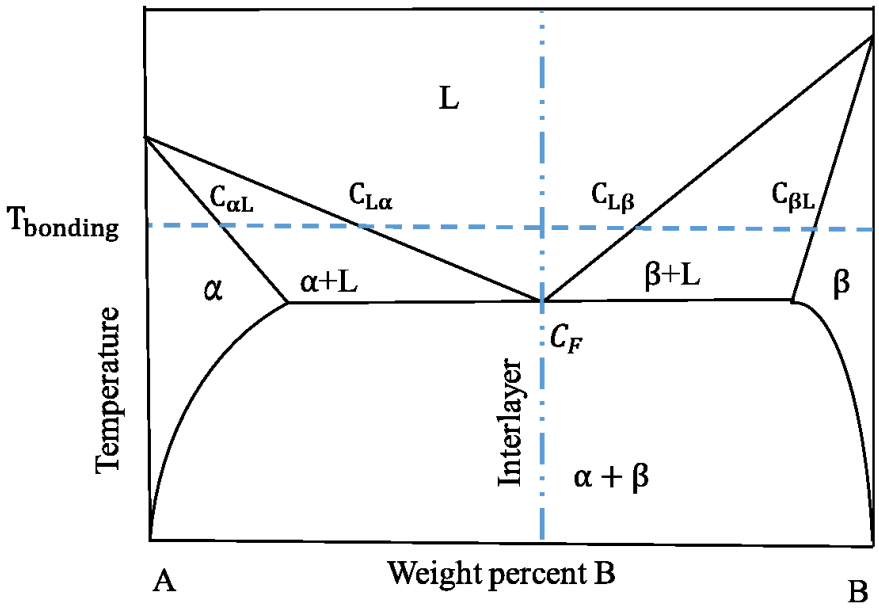

Figure 2: Schematic illustration of the binary eutectic phase diagram.

2.1.2. Heating Stage

At the beginning of the TLP bonding process, the filler alloy and base metals are heated from room temperature to the bonding temperature. During the heating stage, solid-state diffusion of MPD element(s) can take place, which is dependent on many factors such as heating rate, the bonding temperature and the diffusivity of the MPD element(s). If the heating rate is slow, considerable solid-state diffusion of the MPD element(s) can occur during the heating process, which can lead to the loss of the filler alloy after the process. This problem is severe for thin interlayers with low solute concentration [12]. Hence, proper selection of the heating rate and the initial thickness of the interlayer alloy are essential for this stage.

2.1.3. Dissolution Stage

Due to the higher amount of solute in the liquated interlayer than the liquidus and solidus values required to attain equilibrium concentrations, MPD element(s) diffuse into the solid phase during the dissolution process. Hence, to reach equilibrium concentrations at the solid-liquid interface, the regions of the base metals next to the liquid interlayer are dissolved. During this process, the MPD concentration in the filler alloy decreases by increasing the volume of the liquid interlayer. The maximum dissolution width (W_{max}) can be obtained at the end of this stage, when the solute concentrations in the liquid and solid phases at the interface, are equal to the equilibrium solidus and liquidus values $C_{\alpha L}$ and $C_{L\alpha}$ respectively (as shown in Figure 3).

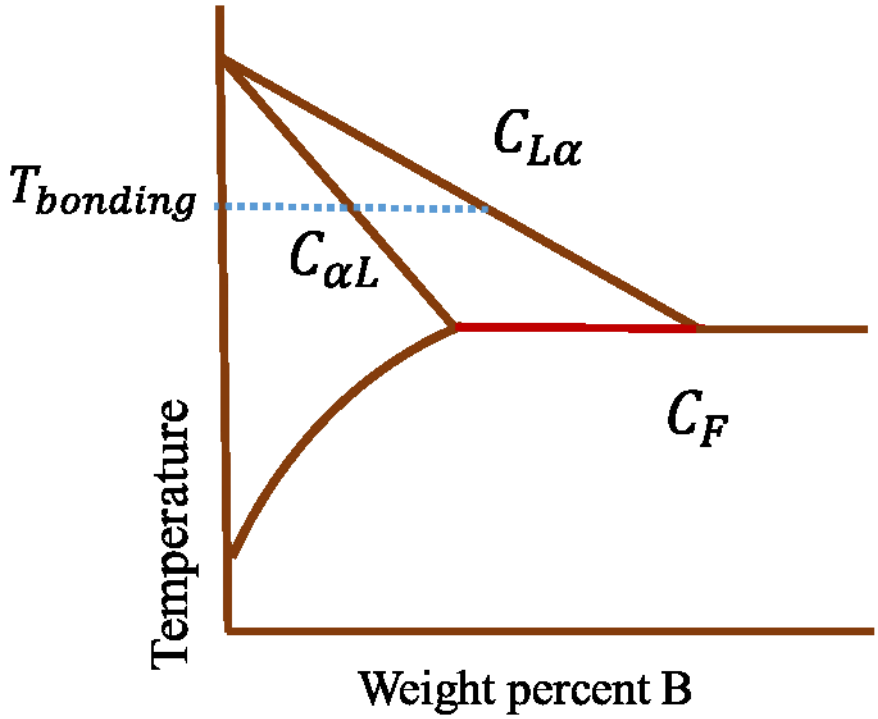

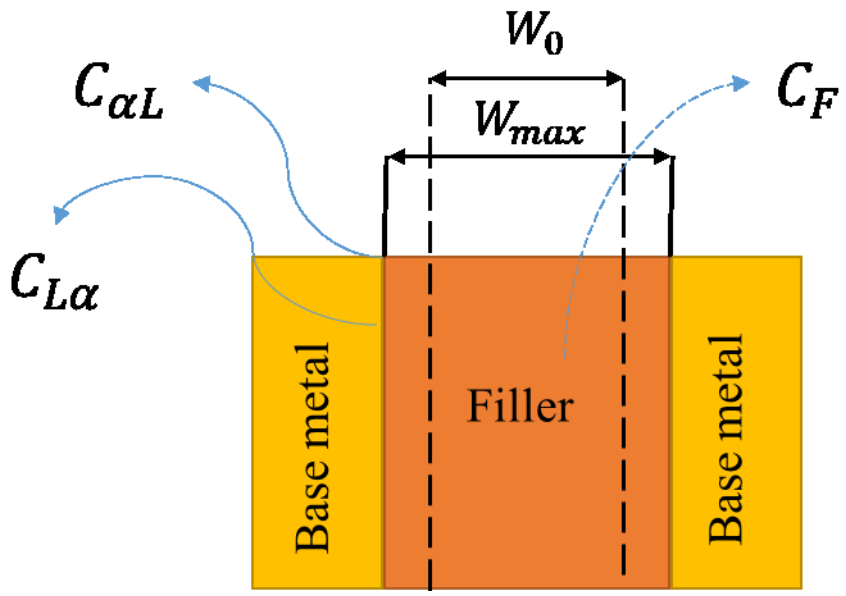

Figure 3: Schematic illustration of the dissolution stage, when the solute concentrations at the interface are equal to the equilibrium solidus and liquidus values.

2.1.4. Isothermal Solidification Stage

After base metal dissolution, the MPD element(s) diffuses further into the base-materials at a constant joining temperature. Due to the loss of MPD element(s), the amount of liquid decreases during the isothermal solidification process, and the liquid-solid interface migrates toward the centerline of the joint. During this process, as shown in Figure 4, the equilibrium solidus and liquidus values remain fixed at $C_{\alpha L}$ and $C_{L\alpha}$ respectively. By providing enough holding time, the liquid phase will completely solidify. Insufficient holding time can result in the transformation of residual liquid interlayer into the eutectic phase, which is very brittle.

Since the isothermal solidification process is controlled by solid-state diffusion of MPD solute into the base metal, it is significantly slower than the heating and dissolution stages. Hence, this stage is the most crucial stage in the TLP bonding process as it requires the most significant amount of time, which may be hours or days [4][14]. Minimizing the time required to complete isothermal solidification can help to reduce fabrication costs. To achieve a successful TLP bonded joint and optimize the processing time, an adequate understanding of the process kinetics is essential.

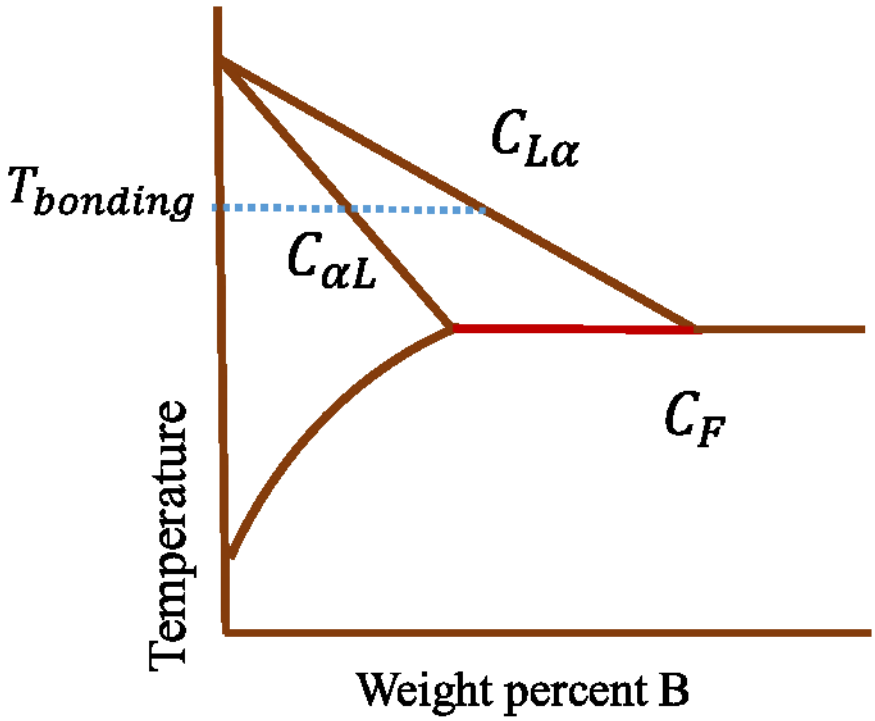

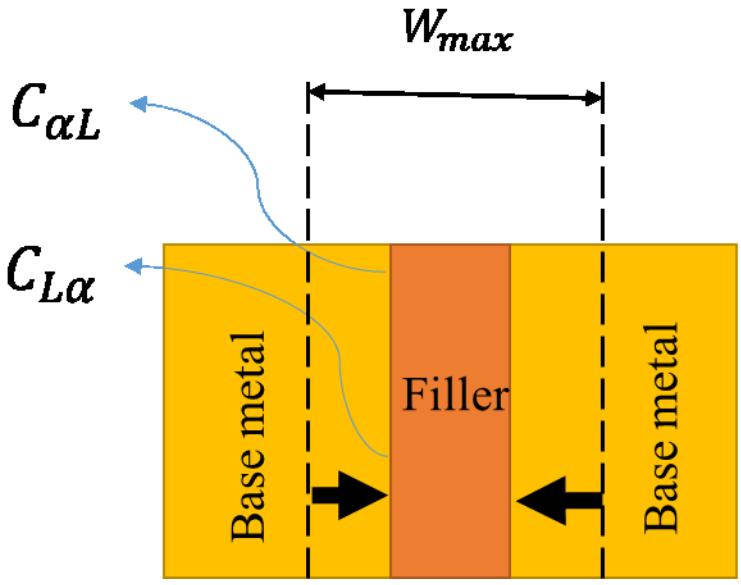

Figure 4: Schematic illustration of the solidification stage, when the solute concentrations at the solid-liquid interfaces, are equal to the equilibrium solidus and liquidus values.

2.1.5. Homogenization Stage

After complete isothermal solidification when the base metals are in contact with each other, there may be high solute concentration in the joint region, which can degrade properties of bonded materials (as illustrated in Figure 5). Therefore, extended holding time may be necessary to continue the solid-state diffusion of MPD solute in order to decrease the maximum concentration of the MPD elements to a specific value to avoid a reduction in material properties [6]. The temperature for this process is usually less than the bonding temperature, especially if the material's microstructures are very sensitive to high temperature [15].

The homogenization process is controlled by a solid-state diffusion similar to the isothermal solidification process. The time that is required to complete homogenization is a function of the required acceptable solute concentration at the centerline of the joint, which may take hours [14]. Since this is one of the effective stages of the TLP bonding processing time, a proper study is needed to better understand the kinetics of this process.

2.2. Important TLP Bonding Parameters

The most crucial factor in TLP bonding is the time required to complete the bonding process with desirable joint properties. Some parameters that affect the kinetics of the TLP bonding process are discussed in this section.

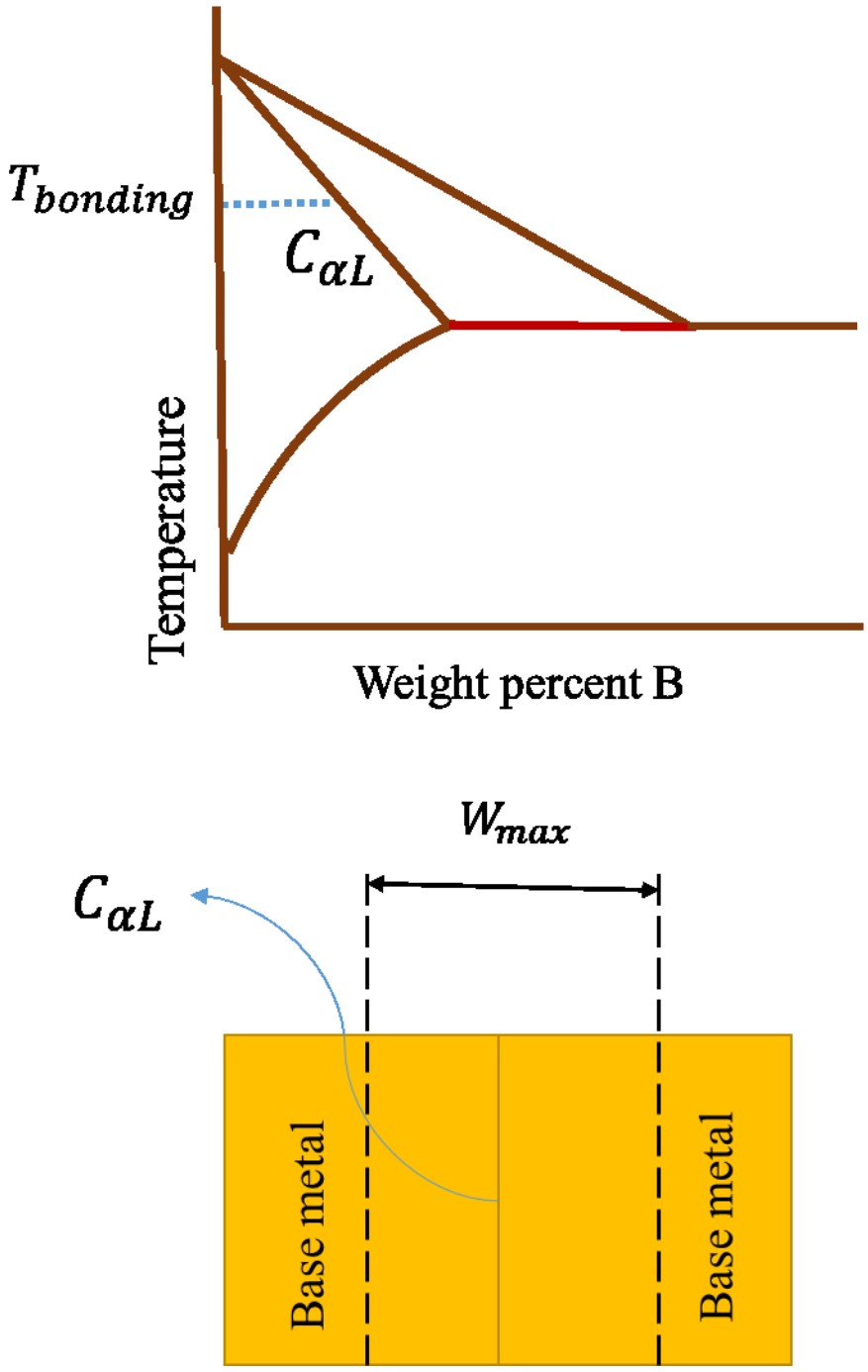

Figure 5: Schematic of initial conditions for the homogenization stage after complete solidification.

2.2.1. Temperature

One of the important parameters in TLP bonding is the bonding temperature. Based on the Arrhenius equation, increasing temperature leads to an increase in diffusivity. Hence, it can be expected that the time required to complete isothermal solidification (t_f) decreases with increasing the bonding temperature. However, by increasing the bonding temperature, it can be observed from the binary alloy phase diagram (as illustrated in Figure 2) that the equilibrium solidus and liquidus values are declining. This decrease in equilibrium solidus and liquidus concentration leads to a decrease in the entire amount of solutes can diffuse into the base metals and decrease the concentration gradient near the solid-liquid interface. Therefore, it can result in an increase the time required to complete TLP bonding. Hence, proper selection of the bonding temperature is necessary to minimize the TLP bonding processing time.

2.2.2. Interlayer Features

There are some crucial factors which are essential for the interlayer selection in TLP bonding. The interlayer alloy, which is known as filler alloy, contains a melting point depressant (MPD) element(s), which is added to decrease the filler alloy's melting temperature. In cases where the interlayer contains more than one MPD element, at least one of the MPD elements must have significant diffusivity and solubility in the base metal at the bonding temperature, which controls the mechanism of the process. The interlayer alloy can be in several forms such as powder, paste or foil. However, the chemical composition of the filler alloy must not degrade the properties of the base metal [4].

Also, the interlayer alloy should have appropriate liquidity for ensuring proper wetting and flow within the joint [16]. Besides, adjustment of interlayer thickness should be considered in the TLP bonding. If the filler alloy is too thin, the MPD element in the filler alloy is entirely consumed by solid-state diffusion during the heating process. In contrast, if the filler alloy is too thick, more liquid will be formed in the dissolution stage and longer holding time will be needed to complete the isothermal solidification process.

2.2.3. Base Metal Type

Most metals can be TLP bonded by using an appropriate interlayer. However, it is necessary to have some specific properties for the base metals. Base metals should be capable of accommodating the MPD solute sufficiently. Also, base metals should have enough thermodynamic stability and strength at the bonding temperature [4][16].

2.3. The Basis of TLP Bonding Modeling

Most of the analytical and numerical TLP bonding models focus on base-material dissolution and isothermal solidification stages of the process. As there is a phase change behavior during these stages, they can be considered as a moving boundary problem. Numerical and analytical models are based on Fick's second law of diffusion as follows:

$$\frac{\partial c(x,t)}{\partial t} = \frac{\partial}{\partial x}\left(D(x,t)\frac{\partial c(x,t)}{\partial x}\right) \qquad \text{Equation 2}$$

Where x is the distance, t is the time, $c(x,t)$ is the solute concentration, and $D(x,t)$ is the diffusivity of the solute during the process.

2.3.1. Analytical Methods

There have been many efforts to find a reliable analytical model for the dissolution and isothermal solidification processes [14][17][18][19][20]. Gale and Wallach [17] studied the dissolution process by using Equation 3, where the solute concentration in the base metal can be calculated.

$$C(x,t) = 0.5C_0\left[\frac{erf(h-x)}{2\sqrt{D.t}}\right] + \frac{erf(h-x)}{2\sqrt{D.t}} \quad \text{Equation 3}$$

In Equation 3, C_0 is the initial solute concentration in the interlayer, D is the diffusion coefficient of the solute in the solid phase, and h is the width of the interlayer metal. However, this equation is based on two major assumptions, which are; semi-infinite solid substrate width and constant diffusivity [17].

Since the dissolution time is much lesser than the time required for complete isothermal solidification, most analytical models are focused on analysis of the isothermal solidification stage [14][18][19][20]. Tuah-Poku et al. [14] used an analytical solution of the Fick's equation [21] to describe solute distribution in semi-infinite substrate with constant surface concentration ($C_{\alpha L}$) as follows:

$$C(x,t) = C_{\alpha L} + (C_M - C_{\alpha L})\text{erf}(\frac{x}{\sqrt{4Dt}}) \quad \text{Equation 4}$$

Where C_M is the initial solute concentration in the base metal, D is the solute diffusion coefficient, x is distance, and t is the processing time. The total solute quantity is calculated as follows [14]:

$$M(t) = 2(C_{\alpha L} - C_M)\sqrt{\frac{D.t}{\pi}} \quad \text{Equation 5}$$

By ignoring the quantity of solute diffused into the base-material during the heating and dissolution processes, the overall amount of solute diffused into the base metal after complete isothermal solidification is represented as follows [14]:

$$C_F W_0 = 4(C_{\alpha L} - C_M)\sqrt{\frac{D.t}{\pi}} \quad \text{Equation 6}$$

Where C_F is the initial solute concentration in the filler alloy, and W_0 is the initial thickness of the filler metal. Therefore, by using Equation 6, the time for complete isothermal solidification based on the analytical solution can be represented by the following equation [14]:

$$t = \frac{\pi}{16.D}.\left(\frac{C_F.W_0}{C_{\alpha L} - C_0}\right)^2 \quad \text{Equation 7}$$

Similar approach without considering the solid-liquid interface movement is also reported by others (e.g., Nakao et al. [19] and Y. Zhou [20]). However, by using a mass balance approach, the solid-liquid interface position ($X(t)$) has been calculated to be proportional to the square root of time that can be shown as follows [18]:

$$X(t) = K\sqrt{4Dt} \quad \text{Equation 8}$$

Where K is a constant value that can be calculated by the following equation [18]:

$$\frac{K(1+erf(K))\sqrt{\pi}}{exp(-K^2)} = \frac{C_0 - C_{\alpha L}}{C_{L\alpha} - C_{\alpha L}} \quad \text{Equation 9}$$

Also, based on Equation 9 concentration distribution in the solid phase can be calculated as follows [18]:

$$C_\alpha(x,t) = C_{\alpha 0} - \frac{C_0 - C_{\alpha L}}{1 - erf(K)} + \frac{C_0 - C_{\alpha L}}{1 - erf(K)} \times erf\left(\frac{x}{2\sqrt{Dt}}\right) \quad \text{Equation 10}$$

Where C_0 is the solute concentration in the filler alloy prior to bonding. These isothermal solidification analytical solutions are based on four main assumptions: 1) a planar diffusion system, 2) a constant diffusivity, 3) a semi-infinite solid phase, and 4) uniform solute concentration in the liquid phase.

2.3.2. Numerical Methods

Analytical models of TLP bonding are generally based on some non-trivial assumptions, such as; there is no solute concentration gradient in the liquid phase, and the base metal is a semi-infinite solid phase. Hence, several researchers have developed numerical models without these simplifications and assumptions [5][6][7][8][13][22]. TLP bonding is a system of partial differential equations for distinct phases with a moving boundary problem (Stefan problem). Calculation of the interface movement and adjusting the newly calculated position to the new coordinate system at each time step is one of the most challenging features of the TLP bonding numerical simulation. Some general approaches have been defined to solve moving boundary problem. The main ones have been classified by J. Crank [23] into three categories as front-fixing, front-tracking, and fixed-domain.

Regarding the front-tracking method, the front position of the moving boundary can be calculated by the Stefan equation for each step point in time. In this method, the mass transfer equations are needed to be coupled with the Stefan condition at each step of interface movement. The shape of discretization can remain constant (fixed grid method) or vary (moving grid method) [23].

In the front-fixing method, the boundary position is fixed, and the interface is tracked by altering the new coordinate system at each time step. H. G. Landau [24] first proposed a transformation method, which was applied in a finite difference scheme by J. Crank [23]. As an example, the transformation of a one-dimensional moving boundary problem can be expressed by the following equation:

$$\xi = \frac{x}{s(t)} \qquad \text{Equation 11}$$

By fixing the boundary at $\xi = 1$ for all time steps, standard relationships can be explained as follows:

$$\frac{\partial u}{\partial x} = \frac{1}{s(t)}\frac{\partial u}{\partial \xi} \qquad \text{Equation 12}$$

$$\frac{\partial^2 u}{\partial x^2} = \frac{1}{(s(t))^2}\frac{\partial^2 u}{\partial \xi^2} \qquad \text{Equation 13}$$

$$\frac{\partial u}{\partial t}\Big)_x = \frac{\partial u}{\partial \xi}\frac{\partial \xi}{\partial t} + \frac{\partial u}{\partial t}\Big)_\xi = -\frac{x}{(s(t))^2}\frac{ds}{dt}\frac{\partial u}{\partial \xi} + \frac{\partial u}{\partial t}\Big)_\xi \qquad \text{Equation 14}$$

By using Equations 12 to 14, partial differential equations can be solved with the moving boundary problem. Furthermore, for two or more dimensions, the front-fixing method is capable of coupling partial differential equations by body-fitted coordinates or isotherm migration method [23]. Because of the high accuracy of this method compared to the front-tracking method, this transformation technique is used in the present study.

The fixed-domain method is generally used when there is an erratic moving boundary. This technique can be applied to complicated shapes that contain several sharp peaks in more than one dimension. This method can be used for the whole domain at once. In some situations, where a model contains several boundary formations with time, such as an inhomogeneous

solidification, solution of the moving boundary problem can be extremely complicated. In such conditions, using previous approaches may introduce excessive complexities into the modeling and make it very difficult to solve. Therefore, the fixed-domain method is the proper method to use for the modeling of these complex conditions, in which the entire system is considered as one computational domain [23]. Since the numerical model in the current study is in one-dimensional space and no merging or splitting of boundaries occurs, there is no reason to develop a model by using the fixed-domain method.

TLP bonding equations needed for the numerical solutions can be illustrated by Equations 15 to 17, in which Equation 15 shows the diffusion of solute in the liquid phase A and Equation 16 shows the diffusion of solute in the solid phase B. Equation 17 describes the interface movement, where $C(x,t)$ is the concentration as a function of position (x) and the time (t), $D_B(x,t)$ and $D_A(x,t)$ are the diffusion coefficients in the solid and liquid phases respectively. $C_{L\alpha}$ and $C_{\alpha L}$ are the equilibrium liquidus and solidus values. Since the dissolution and solidification stages include interface movement as illustrated in Figure 6, Equation 17 can determine the velocity of the moving interface based on mass balance theory.

$$\frac{\partial C(x,t)}{\partial t} = \frac{\partial}{\partial x}\left(D_A(x,t)\frac{\partial C(x,t)}{\partial x}\right) \quad , \quad 0 < x < s(t) \qquad \text{Equation 15}$$

$$\frac{\partial C(x,t)}{\partial t} = \frac{\partial}{\partial x}\left(D_B(x,t)\frac{\partial C(x,t)}{\partial x}\right) \quad , \quad s(t) < x < L \qquad \text{Equation 16}$$

$$D_A\big(c(x,t)\big)\frac{\partial c(x,t)}{\partial x}\Big|_{x=s^-} - D_B\big(c(x,t)\big)\frac{\partial c(x,t)}{\partial x}\Big|_{x=s^+} = [C_{\alpha L} - C_{L\alpha}]\frac{ds(t)}{dt} \ , \ x = s(t) \qquad \text{Equation 17}$$

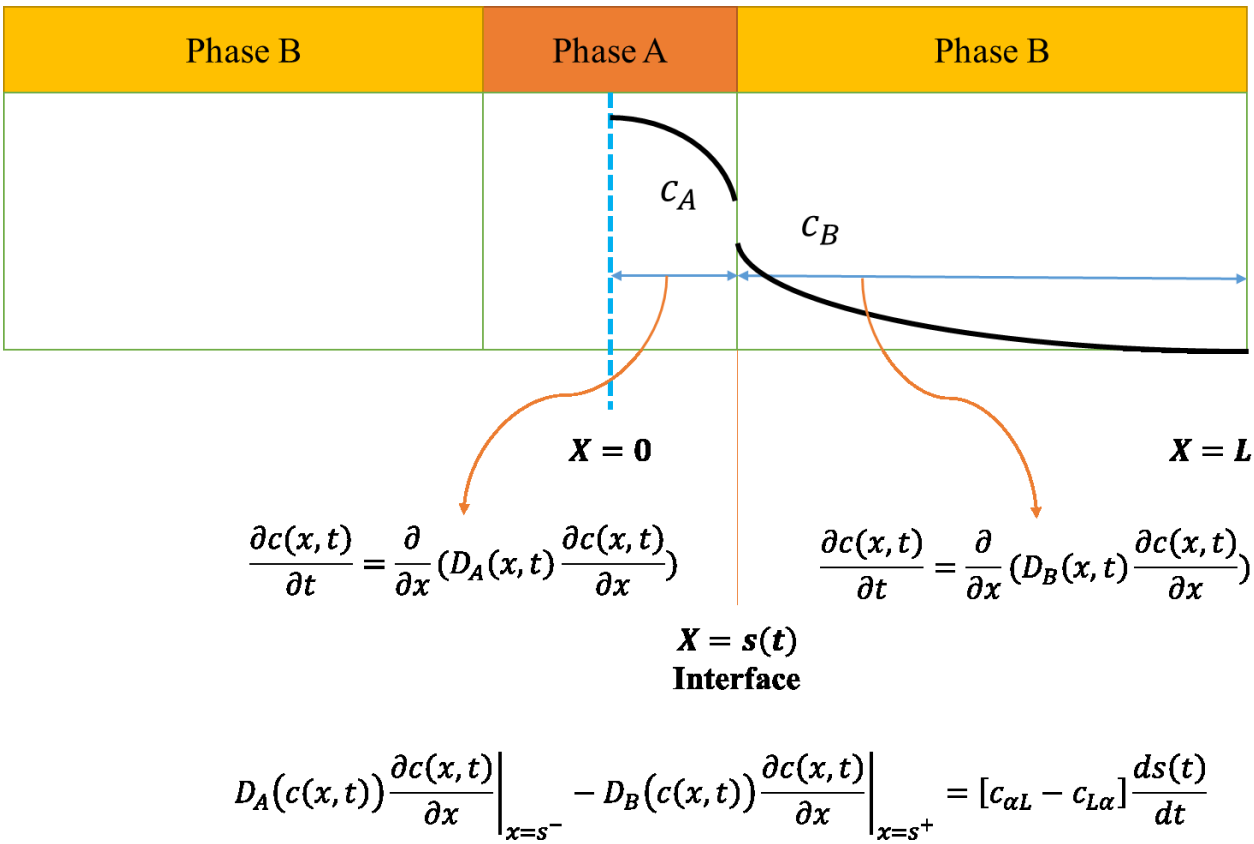

Figure 6: Schematic illustration of diffusion equations of each phase as well as the moving boundary equation.

Nakagawa et al. [7] and Cain et al. [8] solved the diffusion equations at each phase, by discretizing the distance between $x = 0$ and $x = L$ to many fixed grid points. The authors then imposed the interface to be located at one of these prescribed fixed discretization points. Since the interface movement occurs on the fixed grid points, only step-wise motion was allowed. Due to the independency of solute distribution with the interface movement, their approach is not physically feasible. Such a restriction in the interface movement may develop remarkable errors caused by an inaccurate estimation of the interface position [5].

Shinmura et al. [9] developed a numerical TLP bonding model, which was based on tracking the interface position explicitly to predict its motion. In their model, diffusion equations are solved explicitly. By using this approach, Zhou and North [6] developed a model that uses the semi-implicit method, in which the diffusion Equations 15 and 16 are solved implicitly, and the interface diffusion equation has been solved explicitly. In addition, Zhou and North [6] used a front-tracking technique with the capability of tracking the interface between grid nodes. This method has the size of time step limitation, which produces significant errors when large time steps are used. Reduction of the time steps can lead to an increase in computational efforts to solve this problem [5].

Illingworth et al. [5][22] developed a numerical TLP bonding model by using a more accurate discretized scheme for the entire system. They solved the diffusion equations fully implicitly in a one-dimensional system. Also, the front-fixing approach was used for calculating the solid-liquid interface movement, instead of tracking the interface directly. However, diffusivity is assumed to be constant in their model, which cannot be applied for the processes with variable diffusivity.

2.4. Objective of Current Research

As earlier stated in preceding sections, previous TLP bonding models have assumed a process with a constant diffusion coefficient in a planar system to simplify the diffusion equations and the associated moving boundary problem. However, the accuracy of the TLP bonding models based on these non-trivial assumptions is questionable since not all bonding systems have a planar solid-liquid interface and the diffusion coefficient is practically known to vary with composition and even with time. Therefore, the development of a new model with variable diffusion coefficient in planar and non-planar (cylindrical and spherical) systems is crucial to gaining a better understanding of the TLP bonding kinetics. The objective of this study, therefore, is first, to develop a new TLP bonding numerical model with variable diffusivity in planar and non-planar interface systems by using an effective finite difference numerical modeling technique. Secondly, to use the new model to systematically study the effect of variable diffusivity on the isothermal solidification and homogenization kinetics in planar and non-planar systems.

Chapter 3: Development and Validation of a New TLP Bonding Numerical Model

3.1. Model Development

The schematic of the TLP bonding model developed in this research with phase change behavior is shown in Figure 7, in which the concentration of the solute is discretized by many grid points in each phase. An asymmetric system is considered for solving the diffusion equations, while the solid-liquid boundary migrates during the process. Solving the nonlinear diffusion equation with variable diffusivity using the finite difference Crank-Nicolson or fully-implicit methods would require several linear and non-linear assumptions and simplifications, which decrease the accuracy of the model. Using explicit approach for solving the nonlinear diffusion equation makes the model unstable at large time step. Reduction of the time steps can lead to an increase in computational time to solve this problem. Therefore, to prevent using excessive assumptions and instability of the model, an explicit-fully-implicit hybrid method, which is more accurate and reliable for solving complicated nonlinear diffusion equations, is used in this research. Also, Landau transformation technique is applied to conserve the solute in the system, which increase the reliability of the model. The diffusion equation for the liquid phase with a constant diffusivity is solved by using an implicit method similar to the approach used by Illingworth et al. [5]. This is considered valid for the present research because it is generally known that the diffusion coefficient does not vary significantly within the liquid phase. In contrast, however, the diffusion coefficient can vary significantly in the solid phase. Therefore, the new explicit-fully-implicit hybrid solution is developed in the present study, in which an explicit method is used for the solid phase diffusion equation, and a fully-implicit method is used for the diffusion equation in the liquid phase. This makes the model adequately converged and flexible for several boundary conditions.

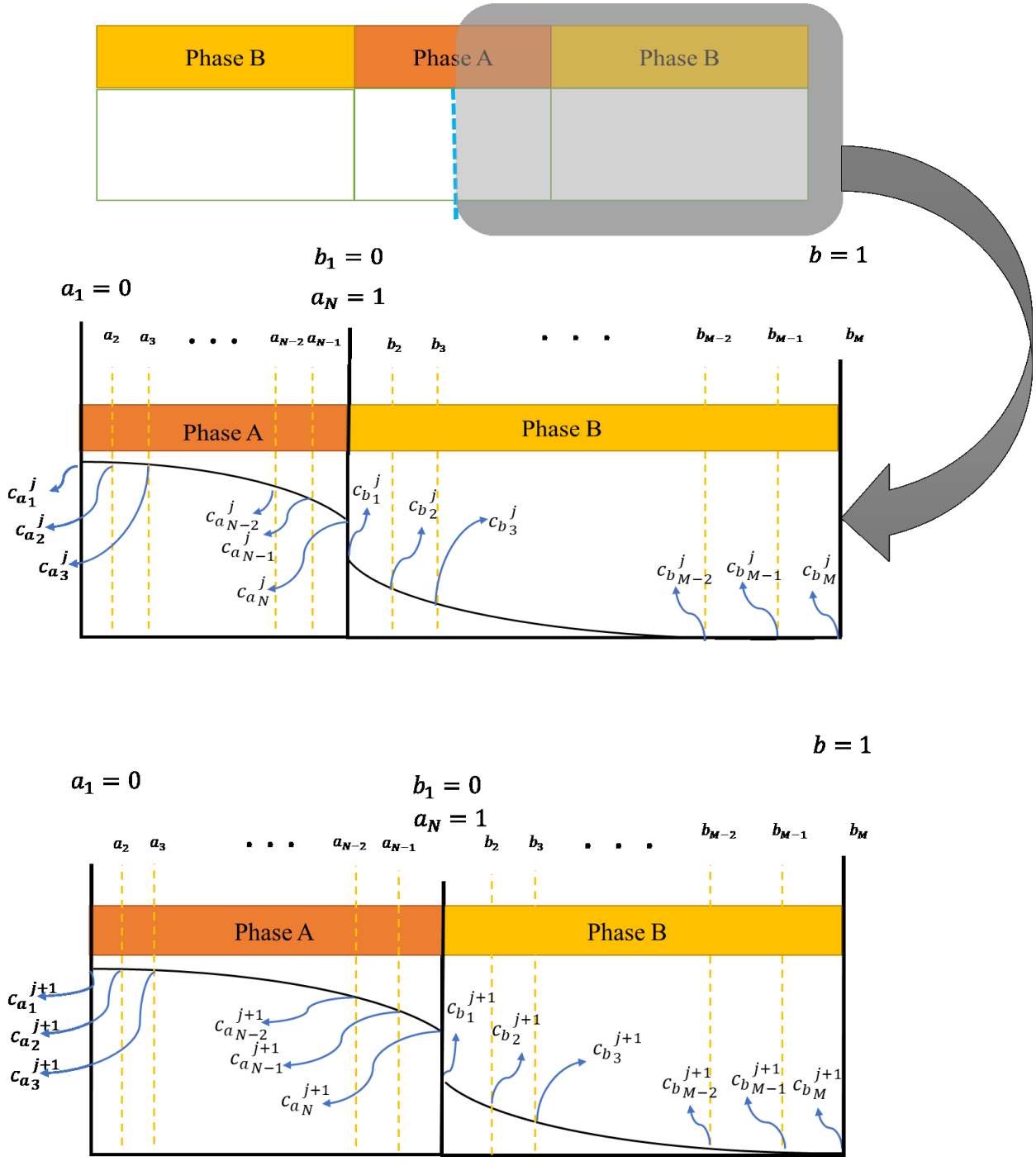

Figure 7: Illustration of the present TLP bonding model scheme based on the Landau transformation for current and future time steps with a moving interface

3.1.1. Dissolution and Isothermal Solidification

As shown in Figure 7, two mass transfer equations are connected to the Stefan equation by the Landau transformation technique, in which the filler alloy is located on the left side of the interface (phase A), and the base metal is located on the right side of the interlayer (phase B). The initial and boundary conditions for the dissolution and isothermal solidification stages can be illustrated as follows:

$$t = 0\,, \quad c(x,0) = \begin{cases} C_A^0, & 0 \le x < s^0 \\ C_B^0, & s^0 < x \le L \end{cases} \qquad \text{Equation 18}$$

$$t > 0\,, \quad c(x,t) = \begin{cases} C_{L\alpha}, & x = s^- \\ C_{\alpha L}, & x = s^+ \end{cases} \qquad \text{Equation 19}$$

Where C_A^0 and C_B^0 are the initial concentrations in phases A and B respectively, and $C_{L\alpha}$ and $C_{\alpha L}$ correspond to the equilibrium concentrations on the surface in the liquid and solid phases respectively. The value of the equilibrium concentrations on the surface for the liquid and solid phases remain constant during the isothermal solidification and dissolution processes.

3.1.1.1. Planar System

The general transformed equation for the liquid phase, based on Fick's second law in a planar system can be written as follows:

$$\left(s^f.\left(C_{a_i}^{\ f}\right) - s^c.\left(C_{a_i}^{\ c}\right)\right).(\Delta a) = (s^f - s^c).\left(C_{a_{i+1/2}}^{\ f}.a_{i+1/2} - C_{a_{i-1/2}}^{\ f}.a_{i-1/2}\right) +$$

$$D_A.\left(\frac{\Delta t}{\Delta a \times s^f}.\left(C_{a_{i+1}}^{\ f} - 2.C_{a_i}^{\ f} + C_{a_{i-1}}^{\ f}\right)\right) \qquad \text{Equation 20}$$

In all the equations in this chapter, superscripts c and f correspond to the current time step and one time step ahead, respectively, subscript i shows the node number, $i-1$ and $i+1$

are nodes before and after the node i respectively. In addition, $i+\frac{1}{2}$ is the node between nodes i and $i+1$ and $i-\frac{1}{2}$ is the node between nodes $i-1$ and i. s^c and s^f show the positions of the interface at the current time step and one time step ahead respectively. $C_{a_i}^{\ c}$ and $C_{a_i}^{\ f}$ are the current and future concentrations at the node i in the liquid phase respectively (the future concentrations are unknown factors in the system). The position of the nodes in local coordinate can be shown as a, where $a_{i+1/2}$ is the local position in the liquid phase between grid points i and $i+1$ and $a_{i-1/2}$ is the local position in the liquid phase between grid points i and $i-1$. In addition, Δa is the distance between 2 nodes in the liquid phase. Δt is the time step and D_A is the diffusion coefficient in the liquid phase. In Equation 20, there are unknown values of concentrations as many as the number of nodes at each time step, which can be calculated with a tri-diagonal matrix.

The procedure developed in this work can be used to analyze any function of concentration dependency of diffusion coefficient, however, power law function is used in this chapter as an example. The general form of the power law concentration-dependent diffusivity is represented by the following equation [25][26]:

$$D_{(c)} = D_0\left(\frac{C}{C_0}\right)^m \qquad \text{Equation 21}$$

Where D_0 is the diffusion coefficient at the specific reference concentration C_0, which in the present work is taken to be the solute concentration in the solid phase at the solid-liquid interface and m is a positive constant as an exponent that can be zero (e.g., $m=0$ shows constant diffusion coefficient). By using Equation 21, diffusion equation for the solid phase can be rewritten by the following equation:

$$\frac{\partial C_{b(x,t)}}{\partial t} = \frac{\partial}{\partial x}\left(D_0\left(\frac{C_b(x,t)}{C_0}\right)^m \frac{\partial C_{b(x,t)}}{\partial x}\right) \quad , \qquad s < x < L \qquad \text{Equation 22}$$

Where $C_b(x,t)$ is the solute concentration in the solid phase B. By applying the Landau transformation method for the solid phase B, the non-linear global equation for concentration distribution is given by the following equation:

$$\left(C_{b_i}^{\ f}.(L-s^f) - C_{b_i}^{\ c}.(L-s^c)\right).\Delta b = (s^f - s^c).\left(C_{b_{i+\frac{1}{2}}}^{\ c}.\left(1-b_{i+1/2}\right) - C_{b_{i-\frac{1}{2}}}^{\ c}.\left(1-b_{i-1/2}\right)\right) +$$

$$\frac{\left(\frac{D_0}{C_0{}^m}\right).\Delta t}{(L-s^c).\Delta b}.\left(\left(C_{b_{i+\frac{1}{2}}}^{\ c}{}^m\right).\left(C_{b_{i+1}}^{\ c} - C_{b_i}^{\ c}\right) - \left(C_{b_{i-\frac{1}{2}}}^{\ c}{}^m\right).\left(C_{b_i}^{\ c} - C_{b_{i-1}}^{\ c}\right)\right) \qquad \text{Equation 23}$$

Where $C_{b_i}^{\ c}$ and $C_{b_i}^{\ f}$ are the current and future solute concentrations at node i in the solid phase B. The position of nodes in local coordinate for the solid phase is shown as b, where $b_{i+1/2}$ is the local position in the solid phase between grid points i and $i+1$ and $b_{i-1/2}$ is the local position in the solid phase between grid points i and $i-1$. Also, Δb is the distance between 2 nodes in the solid phase, and L is the width of base metal plus half-width of filler alloy.

By applying the Landau transformation approach in the Stefan equation, both diffusion equations for the liquid and solid phases can be coupled with the moving boundary equation. Hence, the grid points in each phase can automatically adjust themselves with the interface movement at each time step by using the transformed Stefan equation is given by:

$$s^f = s^c + \left\{\frac{\left(\frac{\Delta t.D_A}{s^c}\right).\left(\frac{C_A - C_{a_{N-1}}^{\ c}}{1-a_{N-1}}\right) - \left(\frac{\Delta t.D_B}{L-s^c}\right).\left(\frac{C_{b_2}^{\ c} - C_B}{b_2}\right)}{C_B - C_A}\right\} \qquad \text{Equation 24}$$

Where $C_{a_{N-1}}^{\ c}$ is the solute concentration at the current time step in the node $N-1$ of the liquid phase A, which is the nearest node to the interface. Cb_2^c is the solute concentration in the

solid phase B at the current time step in the node 2, which is the nearest node to the interface in the solid phase. C_A is the equilibrium concentration in the liquid phase at the interface and C_B is the equilibrium concentration in the solid phase at the interface. All the solutions for the TLP bonding model and algorithms for the simulation are explained in the Appendix.

3.1.1.2. Cylindrical and Spherical Systems

As will be explained in detail in the next sections, for the process in non-planar (cylindrical and spherical) systems, the direction of diffusion can change the TLP bonding behavior. Hence, the TLP bonding models for non-planar systems are developed for two different conditions:

1- The diffusion direction is along the direction of increase in the radius of curvature

2- The diffusion direction is along the direction of decrease in the radius of curvature

Based on condition 1 (phase A is liquid, and Phase B is solid), Equations 25 and 26 can explain the concentration distribution in the liquid and solid phases respectively as follows:

$$\Delta a.\left(C_{a_i}^{\ f}.s^f.((s^f.a_i)^g)-C_{a_i}^{\ c}.s^c.((s^c.a_i)^g)\right)=\Delta t.\Bigg(\left(s^f.a_{i+\frac{1}{2}}\right)^g.\left(\frac{s^f-s^c}{\Delta t}.C_{a_{i+\frac{1}{2}}}^{\ f}.a_{i+\frac{1}{2}}+\frac{D_A}{s^f}.\frac{\left(C_{a_{i+1}}^{\ f}-C_{a_i}^{\ f}\right)}{\Delta u}\right)-\left(s^f.a_{i-\frac{1}{2}}\right)^g.\left(\frac{s^f-s^c}{\Delta t}.C_{a_{i-1/2}}^{\ f}.a_{i-1/2}+\frac{D_A}{s^f}.\frac{\left(C_{a_i}^{\ f}-C_{a_{i-1}}^{\ f}\right)}{\Delta u}\right)\Bigg)$$ Equation 25

$$\Delta b.\left[C_{b_i}^{\ f}.(R-s^f).(b_i(R-s^f)+s^f)^g-C_{b_i}^{\ c}.(R-s^c).(b_i.(R-s^c)+s^c)^g\right]=\Delta t.\Bigg(\left((R-s^c).b_{i+\frac{1}{2}}+s^c\right)^g.\left(\frac{s^f-s^c}{\Delta t}.C_{b_{i+\frac{1}{2}}}^{\ c}.\left(1-b_{i+\frac{1}{2}}\right)+\frac{\left(\frac{D_0}{C_0{}^m}\right).C_{b_{i+\frac{1}{2}}}^{\ c}}{R-s^c}.\frac{\left(C_{b_{i+1}}^{\ c}-C_{b_i}^{\ c}\right)}{\Delta b}\right)-\left((R-s^c).b_{i-\frac{1}{2}}+s^c\right)^g.\left(\frac{s^f-s^c}{\Delta t}.C_{b_{i-\frac{1}{2}}}^{\ c}.\left(1-b_{i-\frac{1}{2}}\right)+\frac{\left(\frac{D_0}{C_0{}^m}\right).C_{b_{i-1/2}}^{\ c}}{R-s^c}.\frac{\left(C_{b_i}^{\ c}-C_{b_{i-1}}^{\ c}\right)}{\Delta b}\right)\Bigg)$$ Equation 26

Where g is the geometry factor that can be 1 and 2 for cylindrical and spherical geometries respectively, and R is the total radius. However, based on condition 2 (phase A is solid, and Phase B is liquid), diffusion equations in the solid and liquid phases are given as follows:

$$\Delta a.\left(C_{a_i}^{f}.s^f.((s^f.a_i)^g)-C_{a_i}^{c}.s^c.((s^c.a_i)^g)\right)=\Delta t.\left(\left(s^c.a_{i+\frac{1}{2}}\right)^g.\left(\frac{s^f-s^c}{\Delta t}.C_{a_{i+\frac{1}{2}}}^{c}.a_{i+\frac{1}{2}}+\frac{\left(\frac{D_0}{C_0{}^m}\right).\left(C_{a_{i+\frac{1}{2}}}^{c}{}^m\right)}{s^c}.\frac{\left(C_{a_{i+1}}^{c}-C_{a_i}^{c}\right)}{\Delta a}\right)-\left(s^c.a_{i-\frac{1}{2}}\right)^g.\left(\frac{s^f-s^c}{\Delta t}.C_{a_{i-\frac{1}{2}}}^{c}.a_{i-\frac{1}{2}}+\frac{\left(\frac{D_0}{C_0{}^m}\right).\left(C_{a_{i-\frac{1}{2}}}^{c}{}^m\right)}{s^c}.\frac{\left(C_{a_i}^{c}-C_{a_{i-1}}^{c}\right)}{\Delta a}\right)\right)$$

Equation 27

$$\Delta b.\left[C_{b_i}^{f}.(R-s^f).(b_i.(R-s^f)+s^f)^g-C_{b_i}^{c}.(R-s^c).(b_i.(R-s^c)+s^c)^g\right]=\Delta t.\left(\left((R-s^f).b_{i+\frac{1}{2}}+s^f\right)^g.\left(\frac{s^f-s^c}{\Delta t}.C_{b_{i+\frac{1}{2}}}^{f}.\left(1-b_{i+\frac{1}{2}}\right)+\frac{D_B}{R-s^f}.\frac{\left(C_{b_{i+1}}^{f}-C_{b_i}^{f}\right)}{\Delta b}\right)-\left((R-s^f).b_{i-\frac{1}{2}}+s^f\right)^g.\left(\frac{s^f-s^c}{\Delta t}.C_{b_{i-\frac{1}{2}}}^{f}.\left(1-b_{i-\frac{1}{2}}\right)+\frac{D_B}{R-s^f}.\frac{\left(C_{b_i}^{f}-C_{b_{i-1}}^{f}\right)}{\Delta b}\right)\right)$$

Equation 28

Therefore, the transformed diffusion equations and the moving boundary equation can be solved simultaneously at each time step to simulate the dissolution and isothermal solidification behavior with variable diffusivity in different geometries.

3.1.2. Homogenization

There are some differences between the isothermal solidification and homogenization stages. First, there is no moving boundary problem in the homogenization stage. Second, the

interface concentration reduces with time during homogenization but is constant during isothermal solidification. Therefore, the following global equation can explain the solute diffusion process during the homogenization stage for a planar system:

$$\left(C_i^f - C_i^c\right).\Delta x = \frac{\left(\frac{D_0}{{C_0}^m}\right).\Delta t}{2}.\left(\left[{C^f_{i+1/2}}^m.\frac{C_{i+1}^f - C_i^f}{x_{i+1}-x_i} - {C^f_{i-1/2}}^m.\frac{C_i^f - C_{i-1}^f}{x_i - x_{i-1}}\right] + \left[{C^c_{i+1/2}}^m.\frac{C_{i+1}^c - C_i^c}{x_{i+1}-x_i} - {C^c_{i-1/2}}^m.\frac{C_i^c - C_{i-1}^c}{x_i - x_{i-1}}\right]\right)$$

Equation 29

Where x is the distance from the centerline of the joint and Δx is the distance between two grid points. Furthermore, the solution for the homogenization process with non-planar interface systems can be represented by the following global equation:

$$r^g_{i+\frac{1}{2}}.\left(c^f_{i+1/2} - c^c_{i+1/2}\right) + r^g_{i-\frac{1}{2}}.\left(c^f_{i-1/2} - c^c_{i-1/2}\right) = \frac{\left(\frac{D_0}{{C_0}^m}\right).\Delta t}{\Delta r^g}.\left[r_{i+\frac{1}{2}}{}^g.{c^m_{i+\frac{1}{2}}}^f.\left(c^f_{i+1} - c^f_i\right) - r_{i-\frac{1}{2}}{}^g.{c^m_{i-\frac{1}{2}}}^f.\left(c^f_i - c^f_{i-1}\right)\right] + \left[r_{i+\frac{1}{2}}{}^g.{c^m_{i+\frac{1}{2}}}^c.\left(c^c_{i+1} - c^c_i\right) - r_{i-\frac{1}{2}}{}^g.{c^m_{i-\frac{1}{2}}}^c.\left(c^c_i - c^c_{i-1}\right)\right]\right)$$

Equation 30

3.2. Validation of the New Numerical Model

In this section, the TLP bonding numerical model developed in this work is validated using experimental and numerical data available in the literature [5][6][25][27]. Zhou et al. [6] reported numerical and experimental results for the TLP bonding of 3 mm thick single crystal nickel alloy (base metal) and a 12.5 μm thick filler metal. In brief, the authors used a filler alloy that contained Ni-19 at.% P and a single crystal base metal (pure Ni). The liquidus and solidus values at bonding temperature are 10.223 at.% P and 0.166 at.% P respectively. The authors

assumed constant diffusion coefficients, $500\,\mu m^2 sec^{-1}$ and $18\,\mu m^2 sec^{-1}$ for the liquid and solid phases respectively. Similarly, Illingworth et al. [5] developed a new numerical TLP model and calculated a maximum liquid thickness of $23.2\,\mu m$ at the end of the dissolution stage using the same conditions.

The comparison of the present numerical model with those of Illingworth et al. [5] and Zhou et al. [6] using the same initial and boundary conditions is shown in Figure 8. The present numerical result is found to be comparable with the previous numerical results. Also, the maximum width of liquid converges with the experimental data, which also demonstrates the accuracy of the model. In addition, the present developed model is used to compute the solute concentration profile when the diffusion coefficient is dependent on concentration through a power law function (Equation 21), and the results are compared to literature data. The model computed results show an abrupt drop in the concentration profile when exponent $m \geq 1$ as presented in Figure 9. Similar behavior is reported by Kass et al. [25] and Wagner [27] when they studied the influence of power law concentration dependent diffusivity on the solute concentration profile in semi-conductor materials diffusion couple. The agreement with the literature reported data shows the reliability of the newly developed non-linear TLP bonding model.

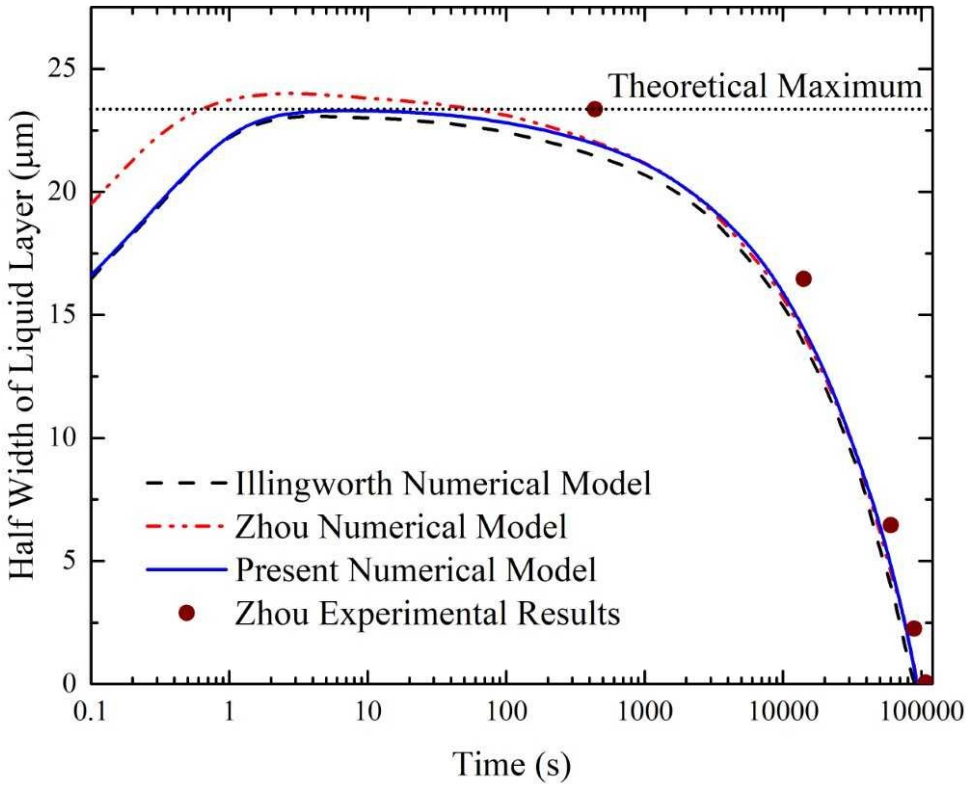

Figure 8: Illustration of the solid-liquid interface movement with time during the TLP bonding process of the Nickel single crystal alloy (as base metal) with Ni-P filler alloy for validation of the present numerical model [5][6].

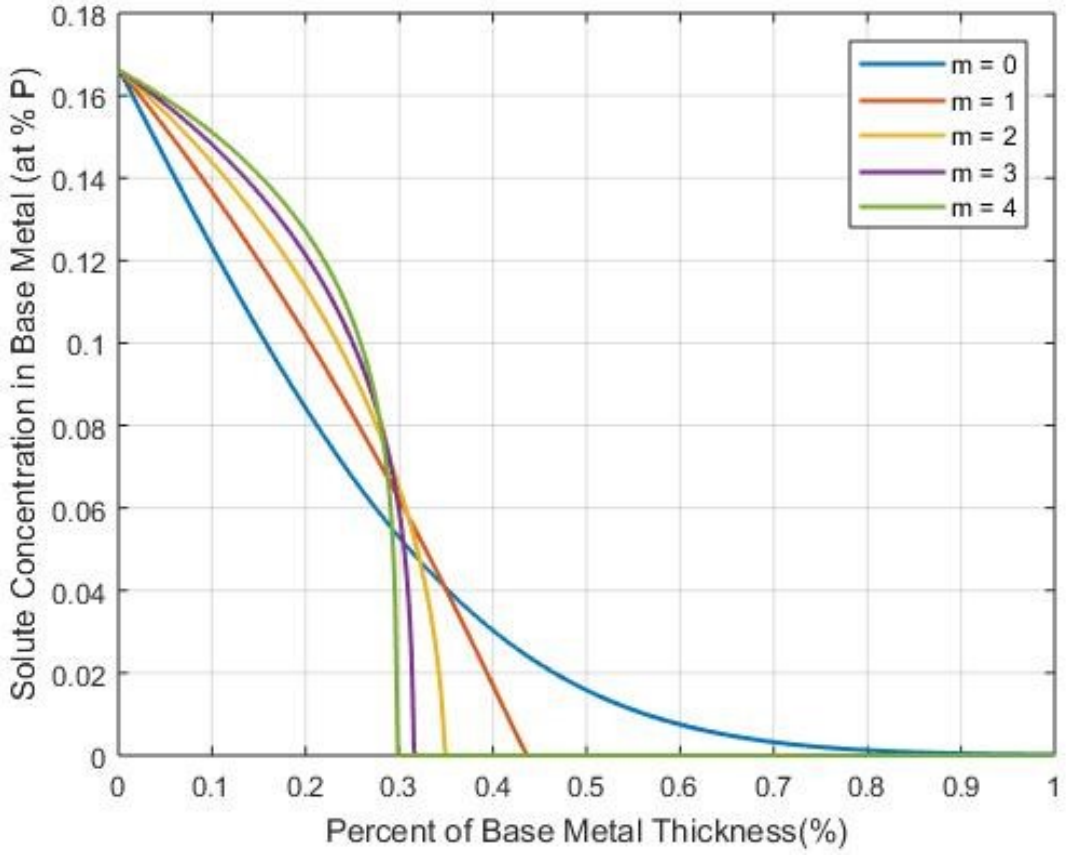

Figure 9: Concentration distribution in the solid phase for the TLP bonding process with power-law concentration-dependent diffusion coefficients (Equation 21) using the new present numerical model. m is the exponent in power form of diffusivity.

Chapter 4: Application of the New Numerical Model

4.1. TLP Bonding Numerical Simulation with Variable Diffusion Coefficients in a Planar System

4.1.1. Effect of Concentration-Dependent Diffusion Coefficients on Isothermal Solidification Kinetics

The kinetics of the isothermal solidification (IS) process is a crucial factor in TLP bonding as it determines the processing time (t_f) required to achieve complete IS and prevent the formation of deleterious microconstituents. Therefore, the main focus of this section is to study the influence of concentration-dependent diffusivity ($D_{(C)}$) on the kinetics of IS and the concomitant time, t_f. Based on the analytical model of TLP bonding, it has been shown that the extent of IS varies linearly with the square root of time ($\sqrt{t}$) and can be represented as follows [18][20]:

$$Y = \emptyset\sqrt{t} \qquad \text{Equation 31}$$

Where Y is the isothermal solidification width and $\emptyset$ is the rate constant. This type of relationship is also known as parabolic law relationship, since Y has a parabolic relationship with holding time. This type of relationship enables the kinetics of the process, at a constant temperature, to be represented by a constant parameter, i.e. by the rate constant $\emptyset$, the slope of the linear plot of Y against $\sqrt{t}$. The practical benefit of having a constant parameter to describe the process kinetics at a given temperature is that it can be readily used to determine how process parameters influence the kinetics and to easily predict the processing time, t_f. Equation 31 is derived based on the condition that when the diffusion coefficient, *D*, is constant and in this case $\emptyset$ is given by [18][20];

$$\emptyset = 2K\sqrt{D}$$ Equation 32

Where K is a function of equilibrium concentrations of the solid and liquid phases at the interface and the initial solute concentration in the filler material (as shown in Equation 9). Therefore, K is a constant at a given temperature and D is the constant diffusion coefficient. A rigorous attempt has been made to use an analytical model to quantify the IS kinetics when D varies with concentration [28]. Their analysis shows that, under the condition of concentration dependent diffusivity, $D_{(C)}$, the extent of isothermal solidification, Y, still varies linearly with $\sqrt{t}$, similar to the case in Equation 31. However, since D is not constant but varies with concentration, the dependency of $\emptyset$, the slope of such linear plot of Y against $\sqrt{t}$, on the variable D, becomes a complicated function that requires a numerical analysis to solve. To understand how the IS kinetics is affected by $D_{(C)}$, it is necessary to determine how $\emptyset$ is influenced by $D_{(C)}$, but this information is not stated in the analytical modeling work reported in the literature. Therefore, in the present work, the new numerical model is used to calculate Y and then and plotted against $\sqrt{t}$ for different forms of $D_{(C)}$. To study how the isothermal solidification kinetics is affected by $D_{(C)}$, three different functions of $D_{(C)}$, through which D increases and/or decreases with increase in concentration are used.

To simulate the case where D increases with increase in concentration, the following equation is used [21];

$$D_{(C)} = D_0.(\frac{C}{C_0})^3$$ Equation 33

The case where D decreases with increase in concentration is simulated by using Equation 34 as follows [21];

$$D_{(C)} = D_0.(\exp(-15.(C - C_0)))$$ Equation 34

To simulate the case where D fluctuates by increasing and decreasing with the increase in concentration, the following equation is used [21];

$$D_{(C)} = D_0.\left(\frac{0.5}{(1-(\frac{C}{C_0})^{0.5}+0.5.(\frac{C}{C_0})^{10}}\right)$$ Equation 35

In all the Equations 33 to 35, D_0 is taken to be the diffusion coefficient on the solid-liquid interface. In addition, the situation where D is constant, independent on concentration, ($D = D_0$) is used as a reference to determine the influence of $D_{(C)}$ on the isothermal solidification kinetics. The results for all the conditions are shown in Figure 10. It is seen from the results that even when D varies with concentration, the IS kinetics can be represented by a constant parameter, $\emptyset$, the slope of the linear plot, similar to the case of constant diffusivity and in agreement with the suggestion by a previous rigorous analytical model [28]. Nevertheless, the numerical analysis performed in this work provides vital additional information on how the kinetics, as defined by $\emptyset$, is affected by $D_{(C)}$. The analysis shows that when D increases with increase in concentration, the process kinetics, as given by $\emptyset$, reduces in comparison with the case of constant diffusivity. However, when D decreases with increase in concentration, the process kinetics, as given by $\emptyset$, increases in comparison with the case of constant diffusivity. In the case where D fluctuates by increasing and decreasing with the concentration, the change in the kinetics as defined by change in $\emptyset$ depends on whether the average of D over the whole concentration range is higher or lower than the case where D is constant. This work, thus, shows that although most analyses of TLP bonding in the literature are done by assuming that D is constant, this is actually a non-trivial assumption, as $D_{(C)}$ affects not only the kinetics, but also the isothermal solidification completion time t_f, as shown by Figure 11.

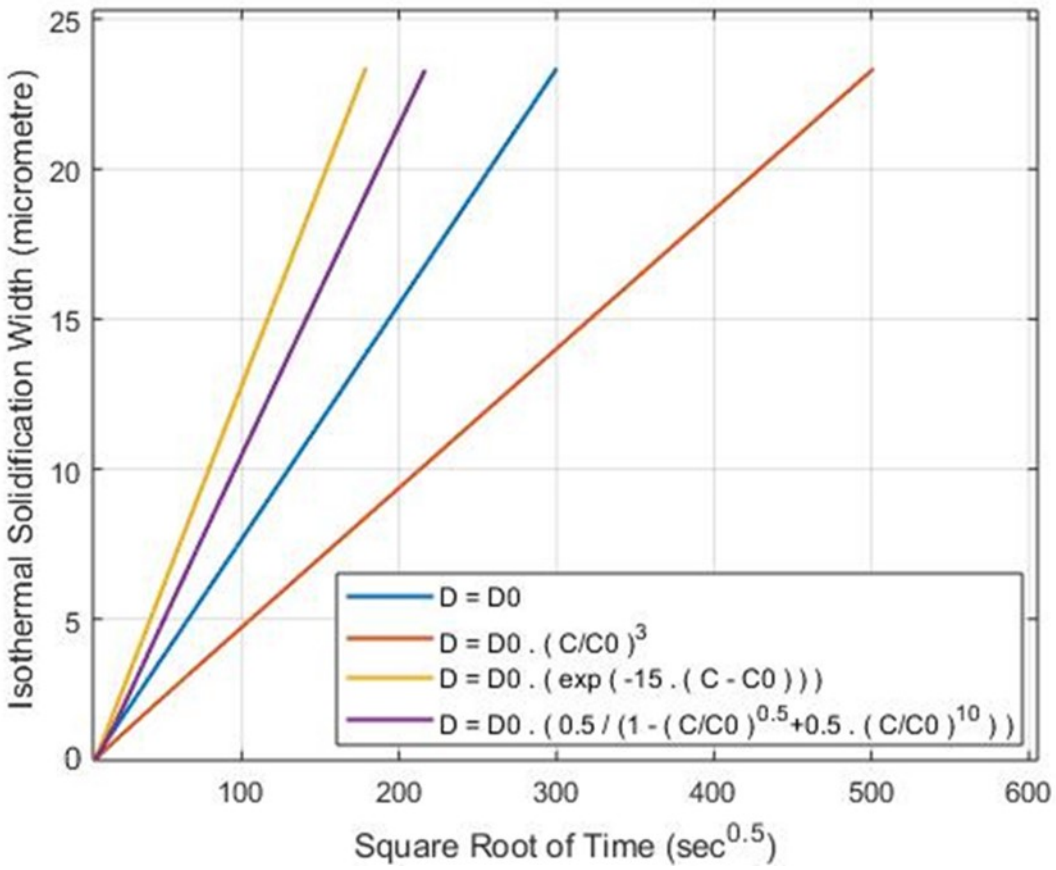

Figure 10: Illustration of isothermal solidification width (Y) and the square root of time ($\sqrt{t}$) for the processes with different forms of concentration-dependent diffusion coefficient ($D_{(C)}$).

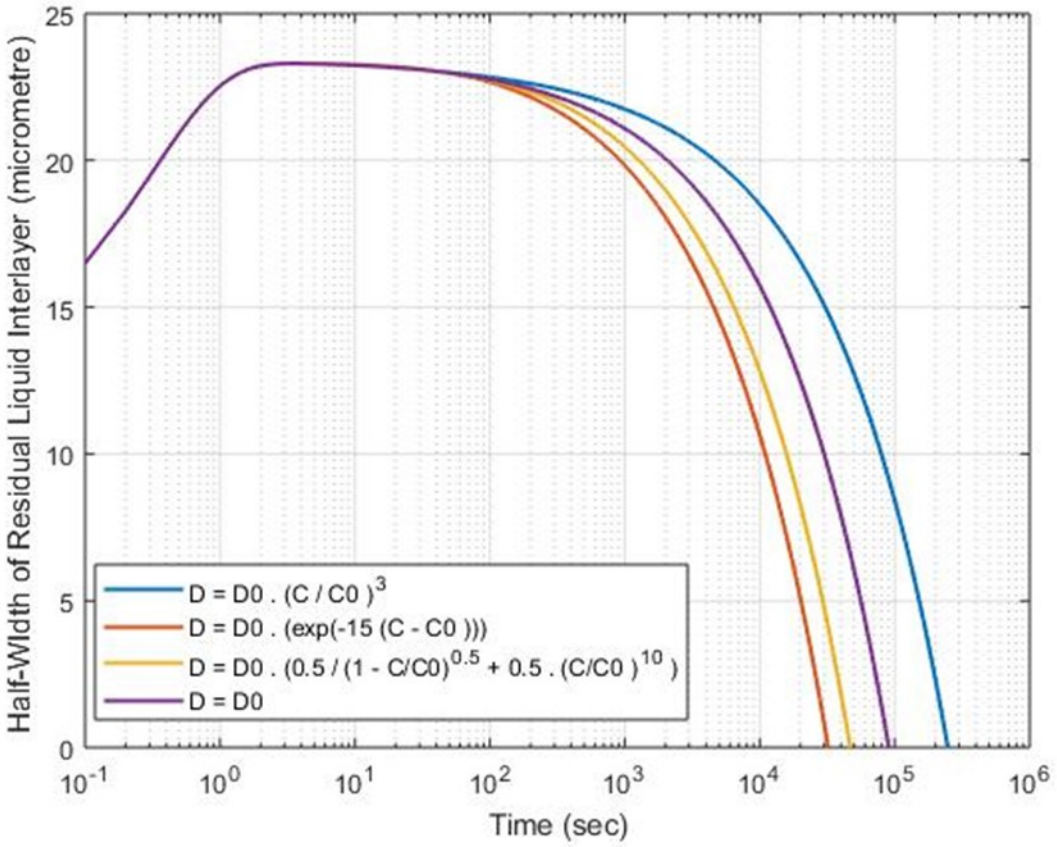

Figure 11: Illustration of the solid-liquid interface migration over time for the TLP bonding process with different forms of $D_{(C)}$.

4.1.2. Effect of Concentration and Time-Dependent Diffusion Coefficient on Isothermal Solidification Kinetics

In the preceding section, the effects of concentration-dependent diffusivity are reported and discussed. It has, however, been found that not only D can vary with concentration, but the concentration dependency of D can actually change with time, although this latter concept is rarely studied in the literature [29]. In this research, four different functions of concentration and time-dependent diffusivity are studied as follows:

$$D(C,t) = D_0 exp(\frac{-t}{P}) exp(m.C) \quad \text{Equation 36}$$

$$D(C,t) = D_0 \left(1 - \frac{t}{t+P}\right) (\frac{C}{C_0})^m \quad \text{Equation 37}$$

$$D(C,t) = D_0 (\frac{C}{C_0})^{m(\frac{t}{t+P})} \quad \text{Equation 38}$$

$$D(C,t) = D_0 (\frac{C}{C_0})^{exp(\frac{t+P}{P})} \quad \text{Equation 39}$$

Where D_0 is the diffusion coefficient at the specific reference concentration C_0, m and P are constant values. Plots of the isothermal solidification width (Y) and half-width of the residual liquid interlayer against $\sqrt{t}$ are presented in Figures 12 and 13 for the processes with a diffusion coefficient that follows Equations 36 to 39. The results show that in comparison to the case where the diffusion coefficient is constant or a function of concentration, the kinetics of isothermal solidification can not be represented by a single rate constant ($\emptyset$) when concentration-dependent diffusivity changes with time ($D_{(C,t)}$). It is seen that when $D_{(C,t)}$, there is a deviation from the linear relationship between Y and $\sqrt{t}$ as well as half-width of residual liquid and $\sqrt{t}$.

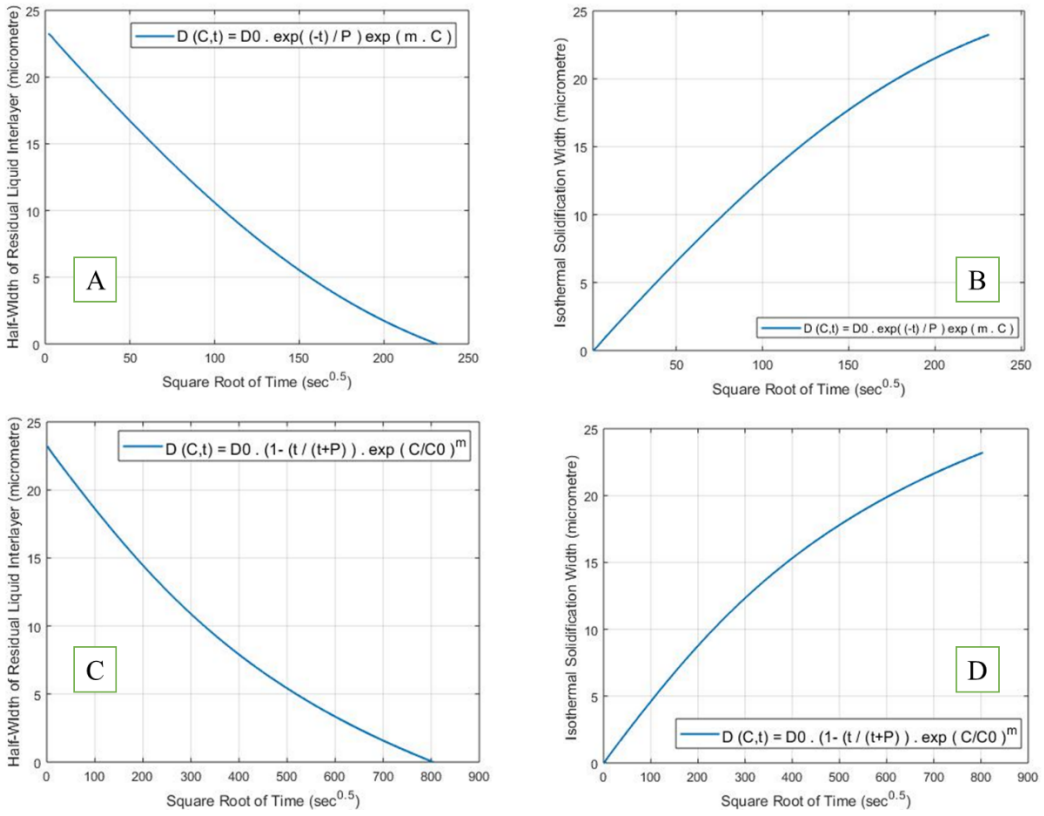

Figure 12: Variation of half width of residual liquid interlayer and Y with $\sqrt{t}$ for the process with concentration and time-dependent diffusion coefficients using Equations 36 and 37 (A and B: $m = 10$ and $P = 40000$, C and D: $m = 3$ and $P = 150000$).

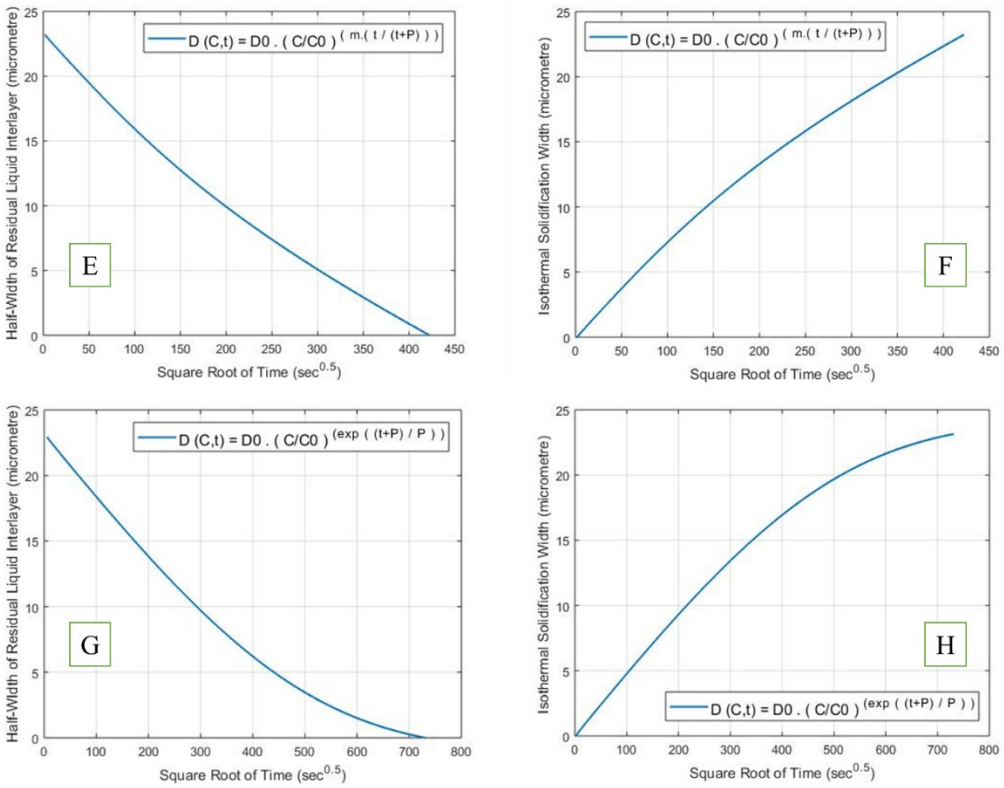

Figure 13: Variation of half width of residual liquid interlayer and Y with $\sqrt{t}$ for the process with concentration and time-dependent diffusion coefficients using Equations 38 and 39 (E and F: $m = 5$ and $P = 100000$, G and H: $P = 190000$).

The deviation from the linear relationship between Y and $\sqrt{t}$ as well as half-width of residual liquid and $\sqrt{t}$ is also called deviation from parabolic behavior between isothermal solidification width and holding time. Although this phenomenon has been experimentally observed and reported by a number of researchers [11][18][30][31][32], no satisfactory explanation has been given for its occurrence. Sinclair et al. [33] suggested that the presence of two MPD elements in the filler alloy, with different diffusivities and/or solubilities in the substrate, can be responsible for the deviation behavior. Nonetheless, the deviation is also observed in a binary system containing one MPD solute [18]. Furthermore, Bai et al. [34] suggested that the formation of second phase precipitates during the isothermal solidification process can cause the deviation from the parabolic behavior. However, Tuah-Poku et al. [14] reported deviation from parabolic behavior in a system where no second phase precipitates form during isothermal solidification. Another researcher, Takenaka et al. [35] reported that grain growth during holding at the bonding temperature is responsible for the deviation behavior. On the contrary, Dinkel et al. [11] and Michael [36] reported deviation in single crystal alloys and polycrystalline metal, respectively, where no grain growth occurs. Michael [36] suggested that a combination of time and concentration dependent diffusivity can cause the deviation. However, the results of the numerical analysis performed in this research show that a mere dependency of D on concentration alone does not produce deviation from the parabolic law. The concentration dependency of D needs to change with time in order for the deviation to occur. This new finding, which has not been reported in the literature, provides a new explanation for the deviation behavior and it can explain its occurrence in systems where suggested reasons provided in the literature do not apply.

Further analysis of this concept in the present work shows that three criteria that can be applied to experimental results to determine if concentration-dependent diffusivity changes with time ($D_{(C,t)}$). The criteria that show that D changes with both concentration and time are listed as follows:

A. Variation in the shape of the solute concentration profiles obtained after different bonding times (Figure 14).
B. Interception of solute concentration profiles that are obtained after different bonding times. As an example, simulated concentration profiles for different bonding times for the case where D depends on concentration by an exponential function $D_{(c)} = D_0 \exp(m.C)$ and where the value of m changes with time, are presented in Figure 15. As seen in the figure, the concentration profiles intercept, which confirms that the concentration dependency of D changes with time. In contrast, when the value of m is constant with time, there is no interception of the profiles as shown in Figure 16.

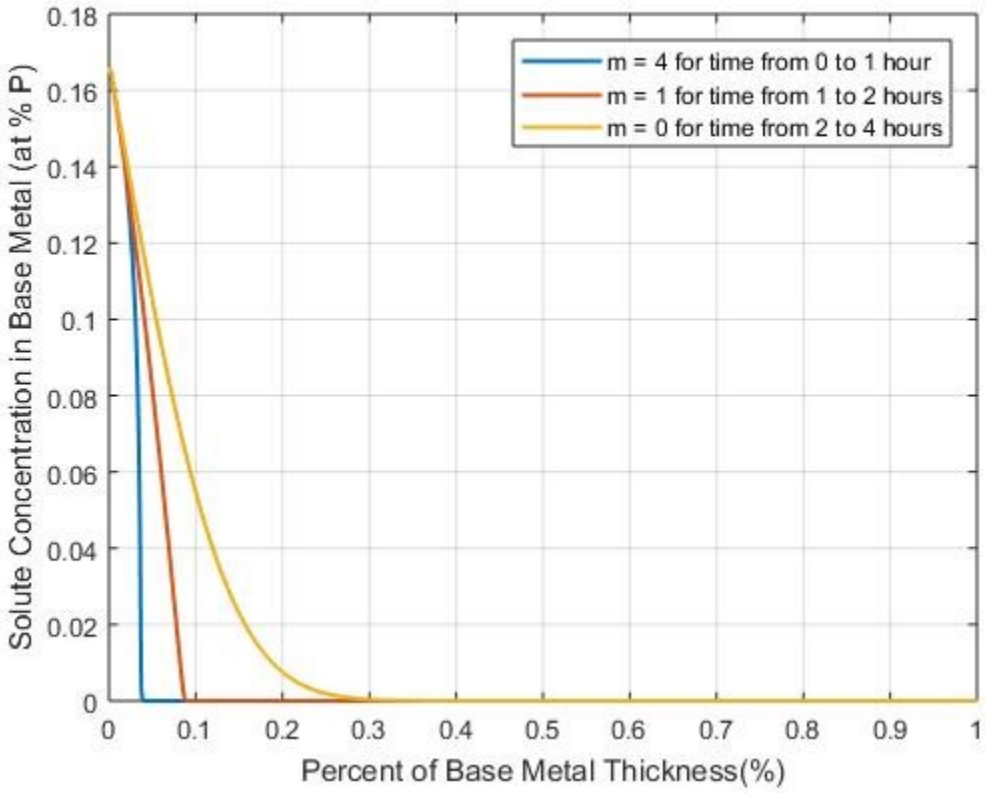

Figure 14: Variation in the shape of the solute concentration profiles obtained after different bonding times when the $D_{(c)}$ is in the power form and the value of exponent m changes with time.

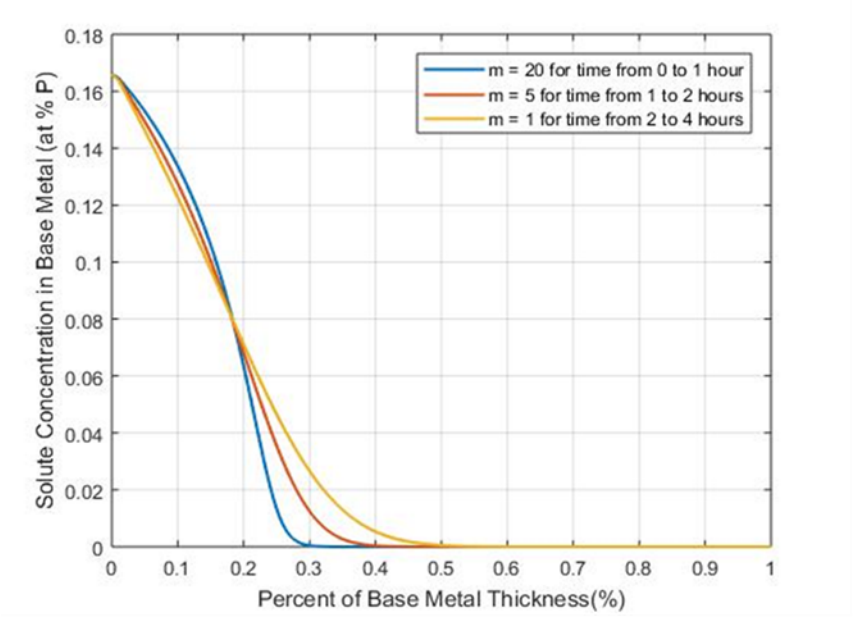

Figure 15: Illustration of interceptions in solute concentration profiles for various processing times when the $D_{(c)}$ is in the exponential form and the value of exponential factor m changes with time.

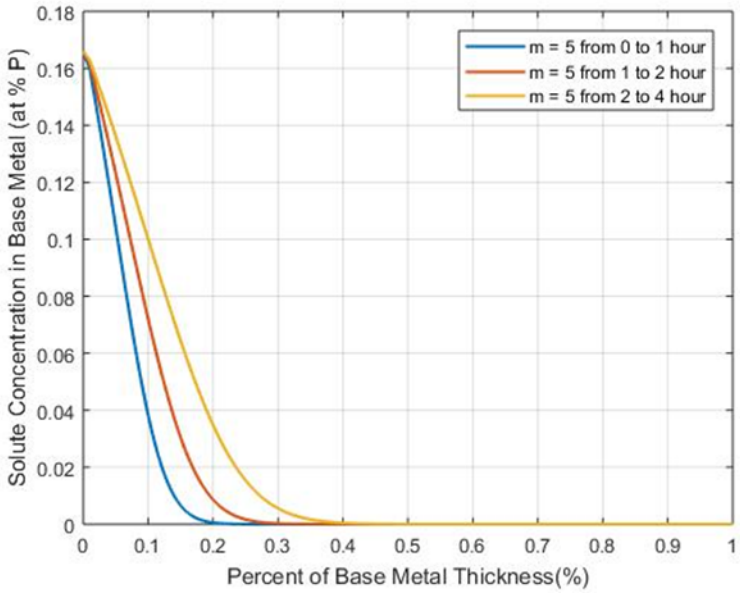

Figure 16: Illustration of solute concentration profiles for various processing times when the $D_{(c)}$ is in the exponential form and the value of exponential factor m is constant with time.

C. Non-coincidence of the end points of all isothermal solute concentration profiles that are obtained after different bonding times, when the profile distance is normalized with respect to $\sqrt{t}$ i.e. when the concentration is plotted against $\frac{x}{\sqrt{t}}$. If D or $F(D_c)$ does not change with time, $\frac{x}{\sqrt{t}}$ normalized concentration profiles for all bonding times will have a common end point. If the end points of all the profiles do not coincide, it shows that the D varies with time. As an illustration, the plots of solute concentration against $\frac{x}{\sqrt{t}}$ after different times for isothermal solidification, for a process where D has a power law concentration-dependency with an exponent $m = 2$ are shown in Figure 17. Since the $F(D_c)$ does not change with time during the process, even though D varies with concentration, all the profiles have a common end point. In contrast, $\frac{x}{\sqrt{t}}$ normalized concentration profiles for a case where D varies with both concentration and time through Equation 38 are presented in Figure 18. As seen in this figure, the end points of all the profiles do not coincide, due to the variation of D with time.

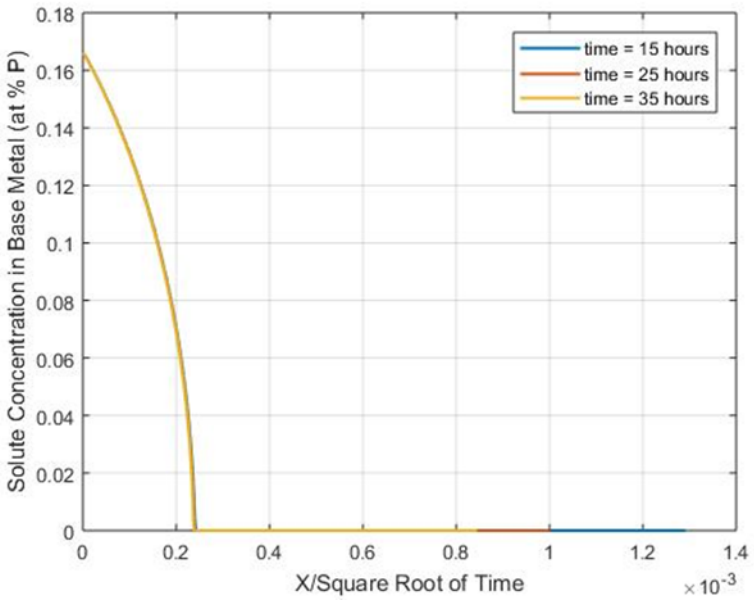

Figure 17: Variation of the solute concentration in the base metal with $\frac{x}{\sqrt{t}}$ for various times, for the process with power form of concentration-dependent diffusivity (Equation 21) with exponent $m = 2$.

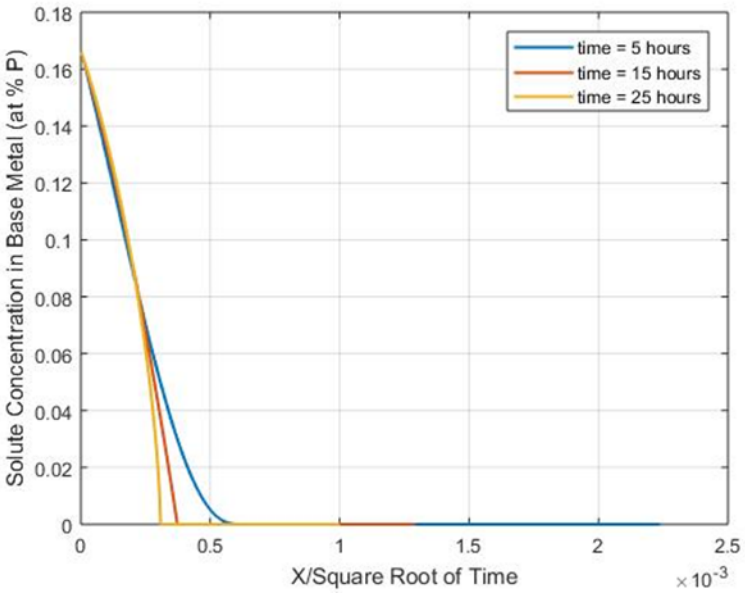

Figure 18: Variation of the solute concentration in the base metal with $\frac{x}{\sqrt{t}}$ for various times, for the process with concentration and time-dependent diffusion coefficient (Equation 38).

In order to use experimental data to verify and confirm a key finding in this research that deviation from the parabolic law behavior is caused by variation in concentration dependency of D with time, the three criteria discussed here are applied to recent experimental results of TLP bonding of Ag with Cu by Michael [36]. Michael [36] observed deviation from the parabolic law during TLP bonding of Ag plates with Cu filler metal at different temperatures. Since only one solute is involved and neither grain growth nor the formation of second phase precipitates are reported to have accompanied the deviation occurrence, the experimental results are well suited to check the validity of the key finding in this research. The experimental results reported by Michael [36] show that;

(i) The shapes of isothermal solute concentration profiles obtained at different holding times differ.

(ii) Some of the isothermal solute concentration profiles obtained at different holding times intercept at some points.

(iii) The end points of various isothermal $\frac{x}{\sqrt{t}}$ normalized solute concentration profiles do not coincide.

These three experimental results listed above confirm the key finding by the numerical analyses performed in this work that deviation from parabolic law can be explained by variation in concentration dependency of D with time. This provides an explanation for the occurrence of deviation even in systems where the existing theorems in the literature do not apply.

4.1.3. Effect of Concentration-Dependent Diffusion Coefficients on the Change in Isothermal Solidification Kinetics with Temperature

One other major factor that is known to affect the isothermal solidification kinetics, as defined by $\emptyset$, is the bonding temperature. Generally, based on Equation 32, temperature can affect $\emptyset$ through its influence on K and D. In the case where D is constant, increase in temperature increases D. At temperatures above the eutectic temperature of some alloy systems, such as, Ni-P, increase in temperature decreases K. In this situation, the change in $\emptyset$ with temperature, i.e. whether it increases or decreases with increase in temperature is determined by a competition between the ratio by which D increases and the ratio by which K decreases. To illustrate this behavior, consider a situation where temperature increases from T_1 to T_2. D_1 and D_2 are diffusion coefficients at T_1 and T_2 respectively, and K_1 and K_2 are the values of K at T_1 and T_2, respectively. The ratio, R_D, by which D_1 increases to D_2 is given by; $R_D = \frac{D_2}{D_1}$ and the ratio, R_K, by which K_1 decreases to K_2 is given by; $R_K = \frac{K_1}{K_2}$. If $R_D > R_K$, $\emptyset$ increases with the increase in temperature and if $R_D < R_K$, $\emptyset$ decreases with the increase in temperature. Values of R_D and R_K at various temperatures in the Ni-P binary alloy system are plotted in Figure 19. As seen from the results, R_D is consistently larger than R_K for all the temperatures from 1100℃ to 1340℃, which leads to increases in $\emptyset$ with increases in the temperature, as shown in Figure 20. Therefore, increase in temperature usually causes isothermal solidification kinetics, as represented by $\emptyset$, to increase. However, the case shown in Figure 20 exists when D is constant. It has been reported in the literature that when D is a function of concentration, the function of the concentration dependency of D, $F(D_c)$, can vary with temperature [37][38].

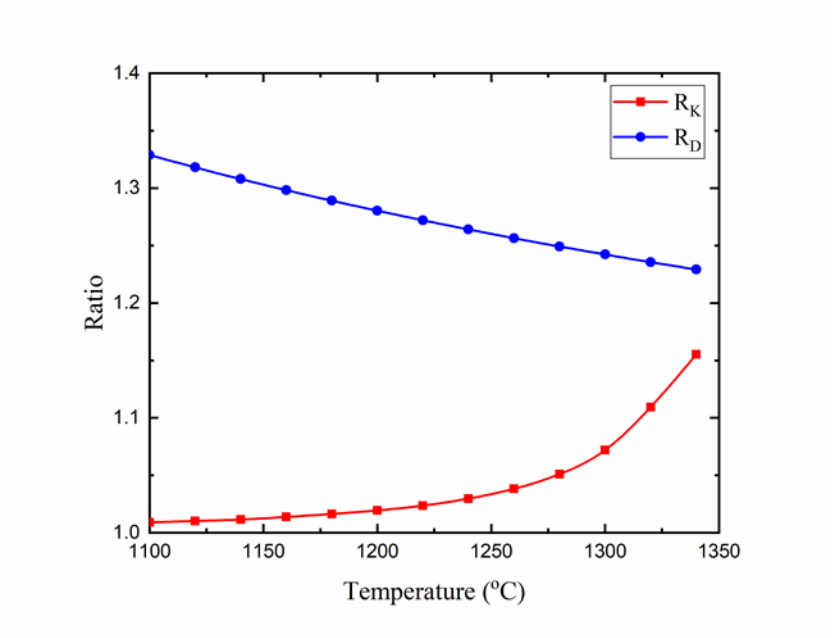

Figure 19: Variation of R_D and R_K by increasing bonding temperature in a Ni-P TLP bonding system with a constant diffusion coefficient.

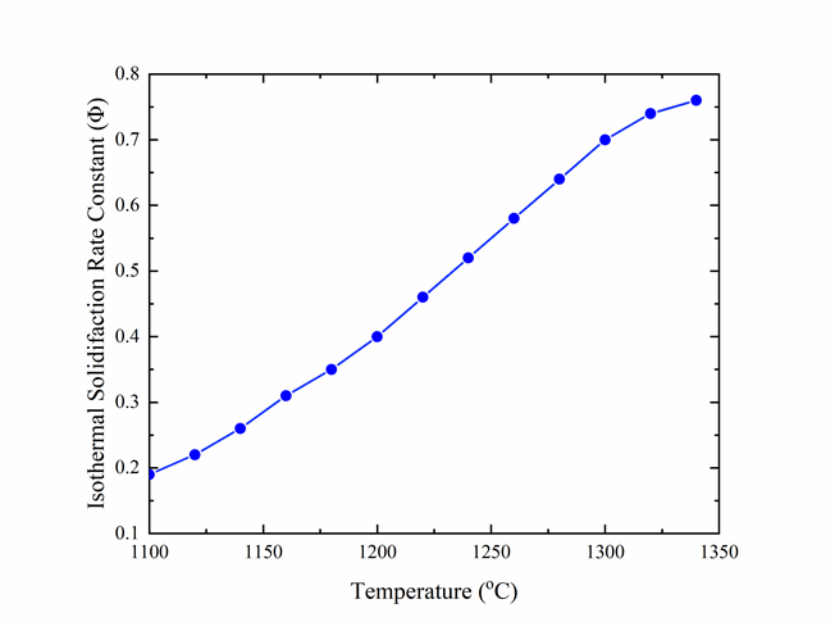

Figure 20: Variation of Ø with increasing temperature for isothermal solidification processes in a Ni-P TLP bonding system with a constant diffusion coefficient.

To study the influence of temperature on $\emptyset$ when D varies with concentration, different cases are investigated in this research, as stated below;

(a) When $F(D_c)$ does not change with temperature

(b) When $F(D_c)$ changes with temperature; two types of this condition are considered.

Power law function based on Equation 21 is used to illustrate the conditions in (a) and (b) above. In the case of condition (b), firstly, the exponent m in the power law function is decreased from 24 to 0 as the temperature is increased and, secondly, m is increased from 0 to 24 with an increase in temperature. The results are presented in Figures 21 to 23 and they show that when $F(D_c)$ does not change with temperature, $\emptyset$ increases with increase in temperature, similar to the case when D is constant. Likewise, when m decreases with increase in temperature, $\emptyset$ increases with increase in temperature. However, when m increases with increase in temperature, $\emptyset$ initially decreases with increase temperature before it increases with further increase in temperature. This result shows that contrary to what is commonly expected, increase in bonding temperature can actually cause the kinetics of isothermal solidification, as represented by $\emptyset$, to reduce. A review of the literature showed a case where experimental results show that $\emptyset$ decreases with increases in temperature but the explanation for the reduction in $\emptyset$ is not provided [11]. The numerical simulations performed in the present research now reveal that it is indeed possible for $\emptyset$ to decrease with increase in temperature if D is concentration dependent and when the associated $F(D_c)$ changes with temperature.

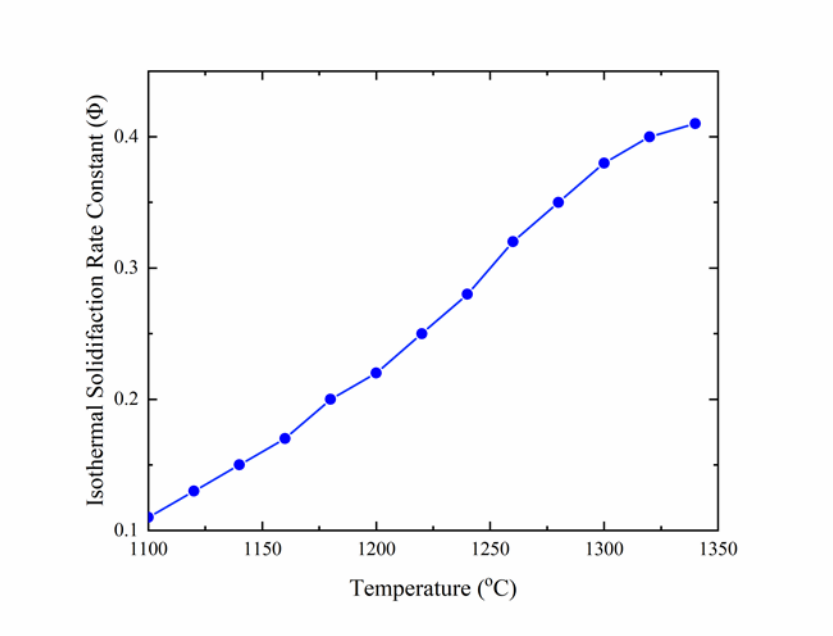

Figure 21: Variation of ∅ with increasing temperature for isothermal solidification processes with power form of $D_{(C)}$, in which exponent is $m = 4$.

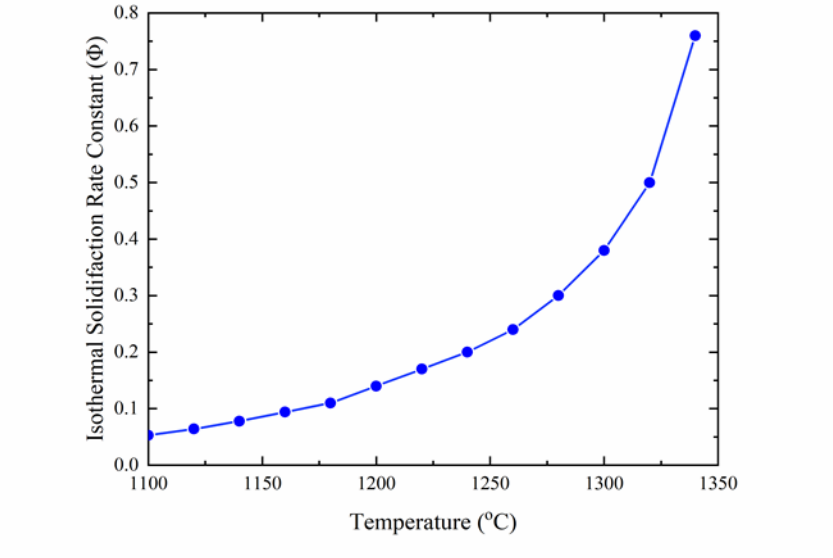

Figure 22: Variation of ∅ with increasing temperature for isothermal solidification processes with power form of $D_{(C)}$, in which the exponent decreases from $m = 24$ to $m = 0$ with increasing temperature.

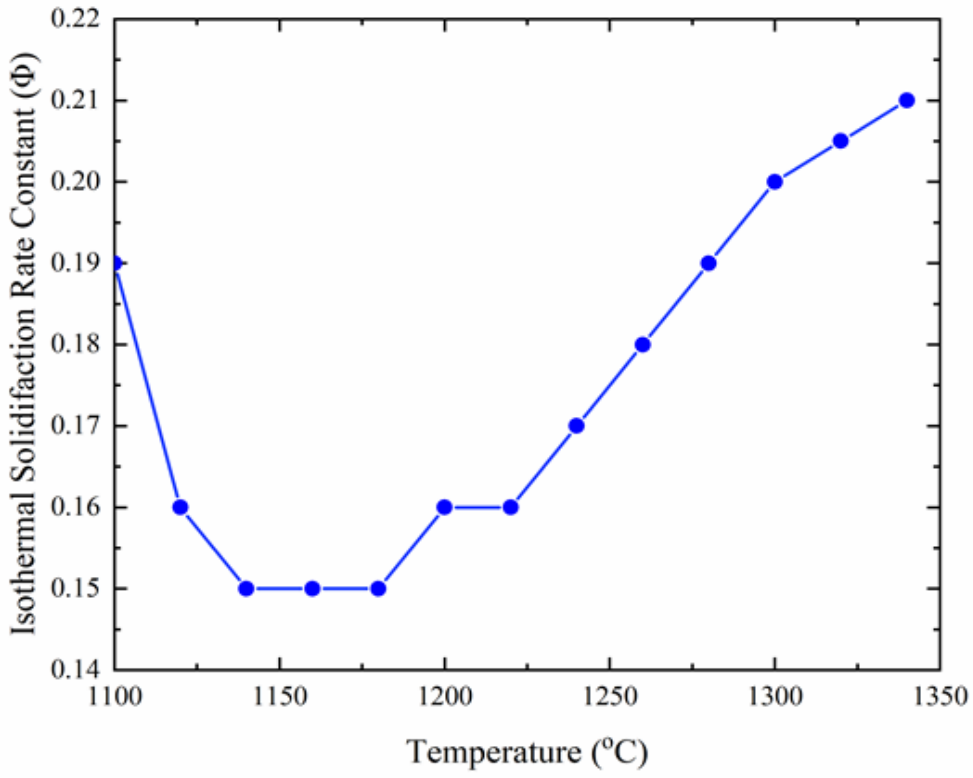

Figure 23: Variation of ∅ with increasing temperature for isothermal solidification processes with power form of $D_{(C)}$, in which the exponent increases from $m = 0$ to $m = 24$ with temperature.

It is also commonly assumed that when the kinetics of isothermal solidification, $\emptyset$, increases with increase in temperature, it will also lead to a reduction in the time t_f required to produce complete isothermal solidification. This is, however, not always the case. It is possible for the kinetics, $\emptyset$, to increase with bonding temperature and the processing time t_f will increase with the increased temperature. This is possible if the increase in the volume of the liquid phase within the joint, due to the base metal dissolution that occurs at the early state of the TLP bonding process, overrides the effect of an increase in $\emptyset$. This is illustrated with the case of TLP bonding of Ni substrate with Ni-P as the filler material. Notwithstanding the increase in $\emptyset$ with an increase in temperature (Figure 20), the processing time t_f increases as the temperature increases (Figure 24) mainly because of the overriding effect of the increased volume of the interlayer liquid as the temperature is increased (Figure 25).

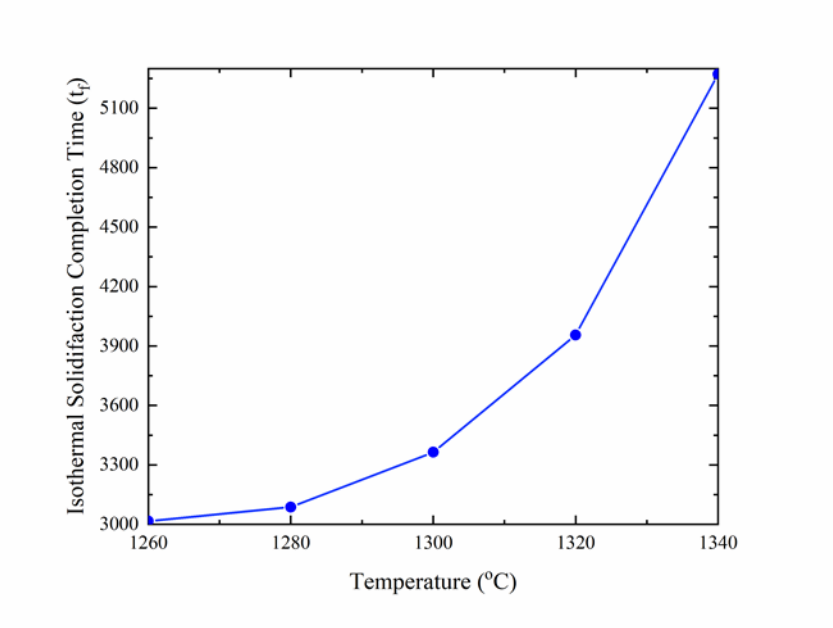

Figure 24: Variation of isothermal solidification completion time t_f with increasing temperature in the Ni-P system.

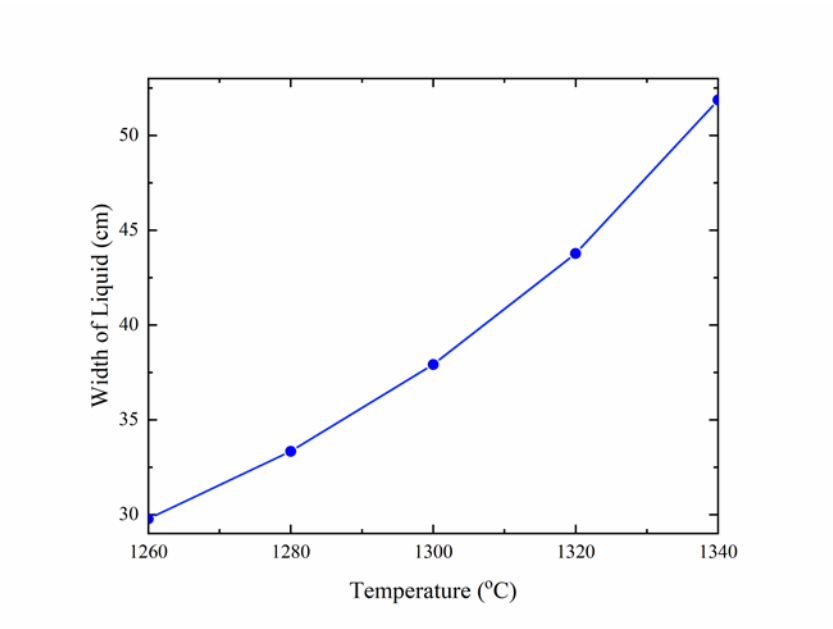

Figure 25: Variation of amount of liquid with increasing temperature in the Ni-P system.

4.2. Effect of Solid-Liquid Interface Geometry on Isothermal Solidification Kinetics

4.2.1. Solid-Liquid Interface Geometry Effect on Isothermal Solidification Kinetics with Constant Diffusivity

Nearly all the cases of TLP bonding reported in the literature involve solid-liquid boundary with planar interface [5][6][7][8][13][22]. Nevertheless, there are several practical situations that involve non-planar solid-liquid interface, for example, bonding of substrate materials with cylindrical and spherical geometries. Therefore, it is crucial to study the influence of geometry on isothermal solidification kinetics and the processing time t_f, even though the mathematics of the non-linear diffusion equations involved significantly are more complicated than those in the planar geometry system. In this section, the influence of non-planarity of the solid-liquid interface on the isothermal solidification kinetics when D is constant is reported and discussed. The case of variable diffusivity is discussed in the succeeding section. In the study of the effects of geometry, two different conditions, A and B, in both the cylindrical and spherical systems are considered as listed below;

Condition A - the diffusion direction is along the direction of increase in the radius of curvature (Figure 26).

Condition B - the diffusion direction is along the direction of decrease in the radius of curvature (Figure 27).

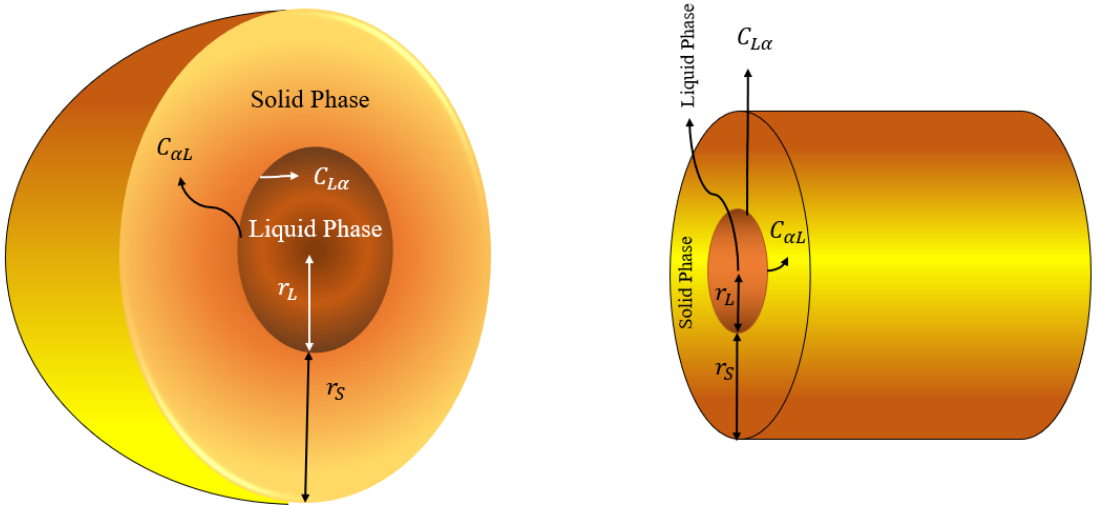

Figure 26: Schematic illustration of cylindrical and spherical systems when the diffusion direction is along the direction of increase in the radius of curvature (condition A).

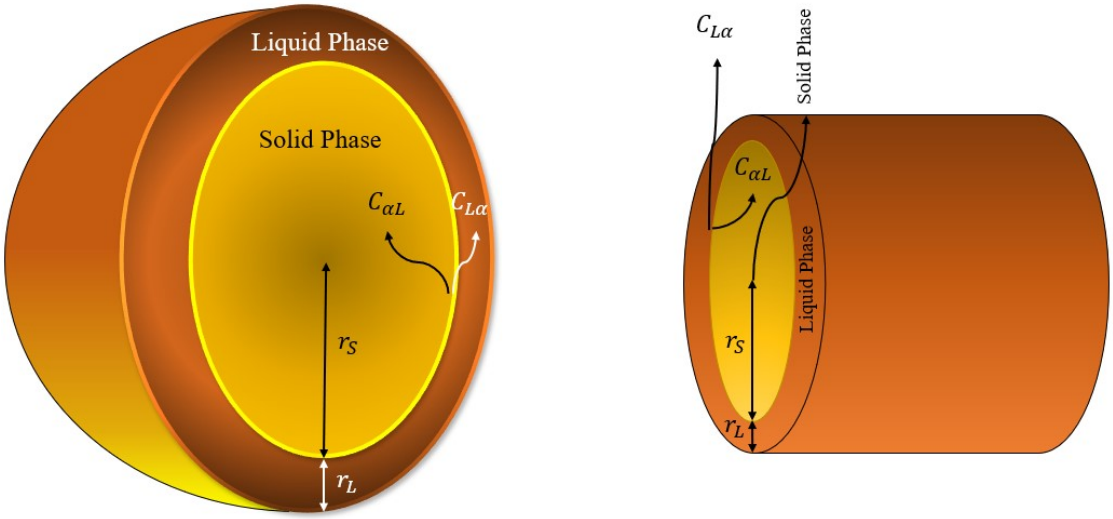

Figure 27: Schematic illustration of cylindrical and spherical systems when the diffusion direction is along the direction of decrease in the radius of curvature (condition B).

The plots of isothermal solidification width (Y) against $\sqrt{t}$ for planar, cylindrical and spherical systems with constant diffusivity are presented in Figure 28. The results show that, in the cylindrical and spherical systems, even though D does not vary with concentration or time, the kinetics of the isothermal solidification process cannot be represented by a constant parameter $\emptyset$. This is because of the relationship between the extent of isothermal solidification and $\sqrt{t}$ deviated from linearity. The extent of deviation is larger in the spherical system compared to the cylindrical system. This is in contrast to the case of a planar system with constant D, where a linear relationship holds between Y and $\sqrt{t}$. Furthermore, in a planar interface system, the location of the liquid relative to the solid-liquid interface does not affect the kinetics of isothermal solidification. However, in non-planar systems, the location of the liquid phase relative to the curved interface profoundly affects the kinetics of the process. There are two types of deviation from the parabolic law relationship in the non-planar interface systems:

1- The deviation is positive i.e. the slope of the curves, $\emptyset$, increases with time when the diffusion direction is parallel to the direction of increase in radius of curvature

2- The deviation is negative i.e. the slope of the curves, $\emptyset$, decreases with time when the diffusion direction is opposite to the direction of increase in radius of curvature

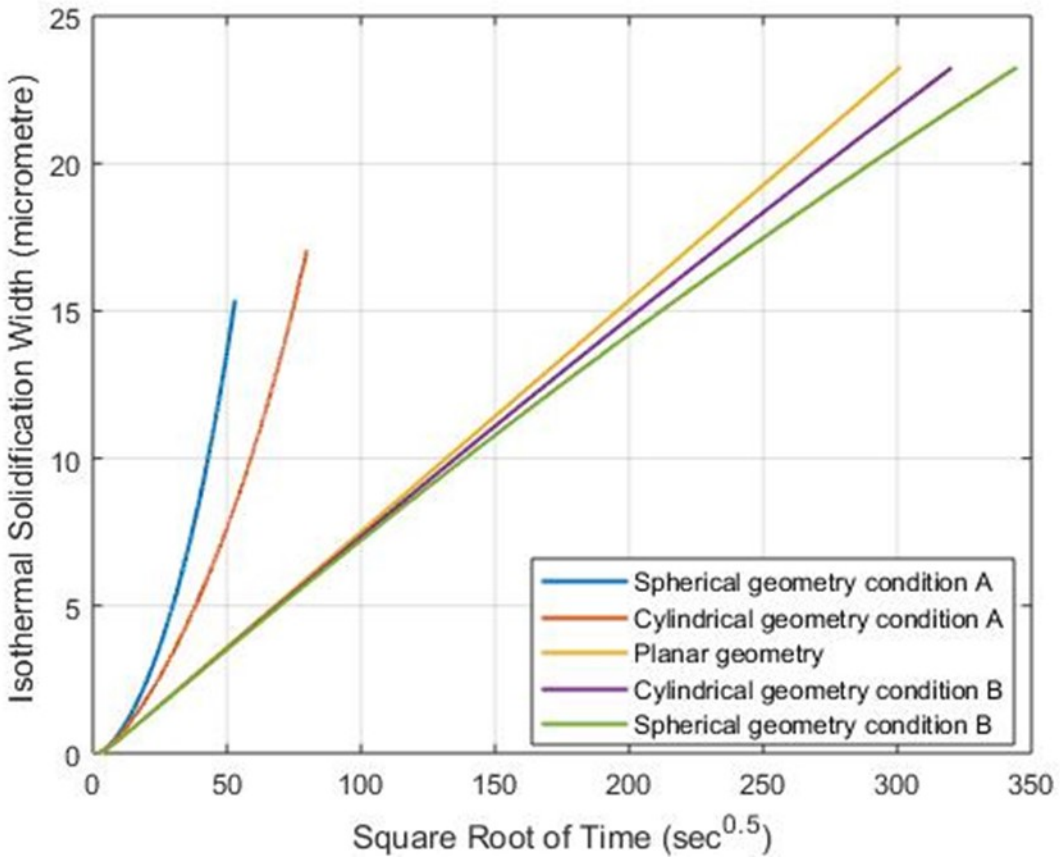

Figure 28: Numerically simulated variation of isothermal solidification width with the square root of time for planar and non-planar systems with a constant diffusivity, for two conditions: A- The diffusion direction is along the increase in the radius of curvature, B- The diffusion direction is along the decrease in the radius of curvature.

The difference between the kinetics of isothermal solidification in the planar and non-planar systems is primarily due to the fact that while the solid-liquid interface movement in the planar system is not accompanied with a change in the interfacial area, the area of the solid-liquid interface in the non-planar systems changes as the interface migrates. The extent of the geometry-induced deviation (G_{dev}) is influenced by the ratio of the instantaneous radius of solid-liquid interface curvature (r) to the initial radius of solid-liquid interface curvature (r_0), i.e.:

$$G_{dev} = \frac{r}{r_0}$$ Equation 40

The different types of deviation, positive and negative, in conditions A and B, are attributable to the difference in the nature of G_{dev} for these two cases. No TLP bonding data on the effects of the cylindrical and spherical solid-liquid interface on isothermal solidification kinetics are found in the literature. Nonetheless, experimental results of diffusion-controlled interface migration [39][40] with similar initial and boundary conditions to those used in this research show that positive and negative deviations occur under conditions A and B, as predicted by the numerical analysis in this work. Any parameter that changes G_{dev}, such as filler alloy thickness can alter the geometry-induced deviation in non-planar systems. Aside from the kinetics of the isothermal solidification process, the non-planar solid-liquid interface also alters the processing time t_f depending on the location of the liquid relative to the curvature of the solid-liquid interface, as shown in Figures 29 and 30.

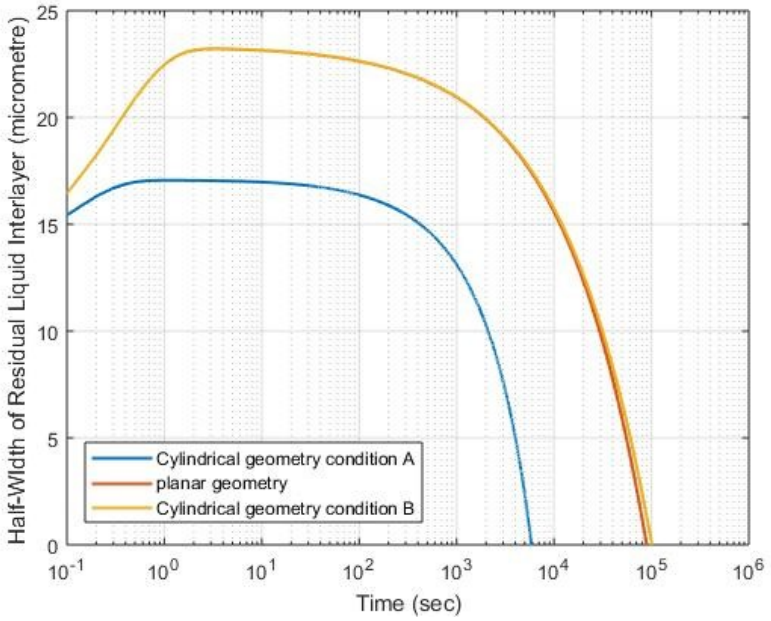

Figure 29: Illustration of the complete isothermal solidification time (t_f) in the process with the cylindrical interface in two different conditions A and B.

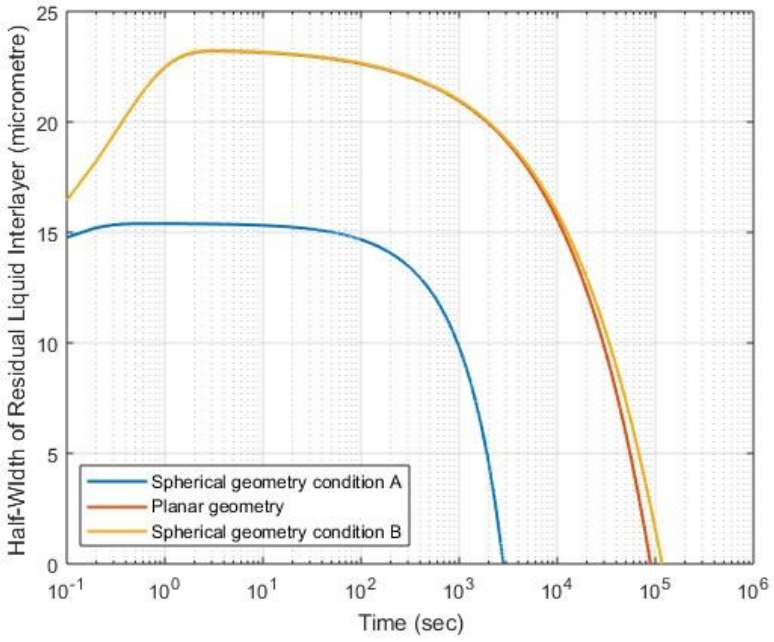

Figure 30: Illustration of the complete isothermal solidification time (t_f) in the process with the spherical interface in two different conditions A and B.

4.2.2. Effect of Substrate Thickness

Another significant difference between isothermal solidification kinetics in planar and non-planar systems is the effect of the size of the solid substrate material that is being bonded. In the planar system, as long as the diffusing solute does not reach the end of the substrate, the size of the substrate does not affect the kinetics of isothermal solidification (Figure 31). This is, however, not the case in non-planar systems. When the direction of the solute diffusion is opposite to increase in the radius, size of the base metal can influence the kinetics of isothermal solidification, even when the solute does not reach to the center of the base metal. This behavior is illustrated in Figure 31 for the process in cylindrical and spherical systems with a constant diffusion coefficient. It can be observed that decreasing the thickness of base metal leads to an increase in the extent of geometry-induced deviation from parabolic behavior in cylindrical and spherical systems. Hence, by decreasing the base metal thickness, isothermal solidification rate constant ($\emptyset$) decreases. This behavior is caused by an increase in the G_{dev} due to a reduction in the thickness of the base-material. In the condition that the diffusion direction is along the increase in the radius of curvature, the thickness of the base metal does not affect the G_{dev}. Hence, in this condition, the base-material thickness does not affect the extent of geometry-induced deviation.

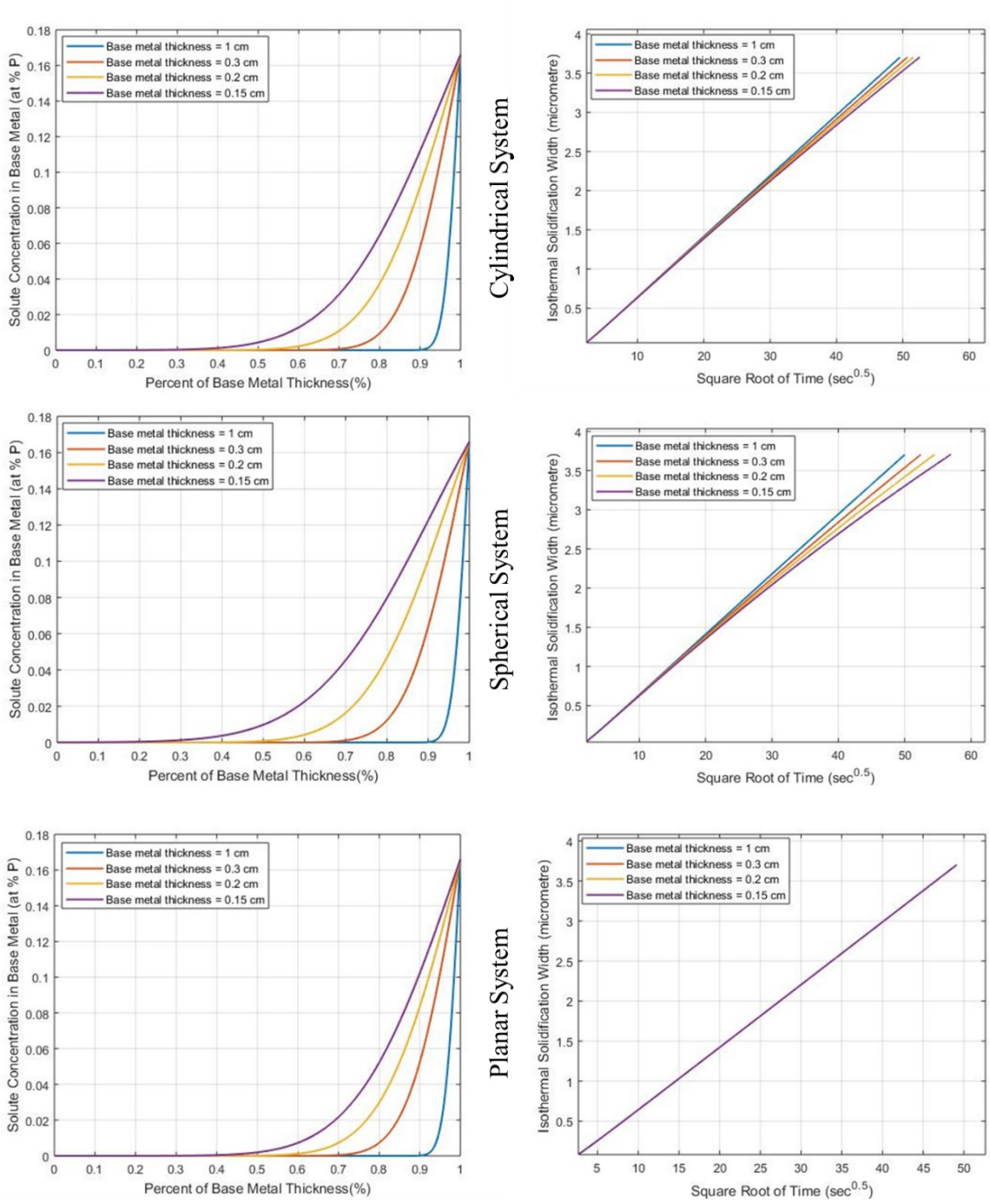

Figure 31: Effect of the substrate thickness on the geometry-dependent deviation from parabolic behavior in cylindrical and spherical interface systems compared to the planar system.

4.2.3. Effect of Variable Diffusion Coefficient on the Isothermal Solidification Kinetics in Non-planar Systems

The effect of variable diffusion coefficients on the kinetics of isothermal solidification is studied in the non-planar systems. A diffusion coefficient with power law concentration dependency (Equation 21) is selected as an example. As presented in Figure 32, variation of D with concentration results in deviation from the parabolic behavior. However, when the concentration dependency of D changes with time, the extent of the deviation increased, as illustrated in Figure 32. Hence, when the diffusion coefficient is a function of concentration and time in non-planar systems, deviation from the parabolic behavior occurs due to the geometry effect and variation in the concentration dependency of D with time.

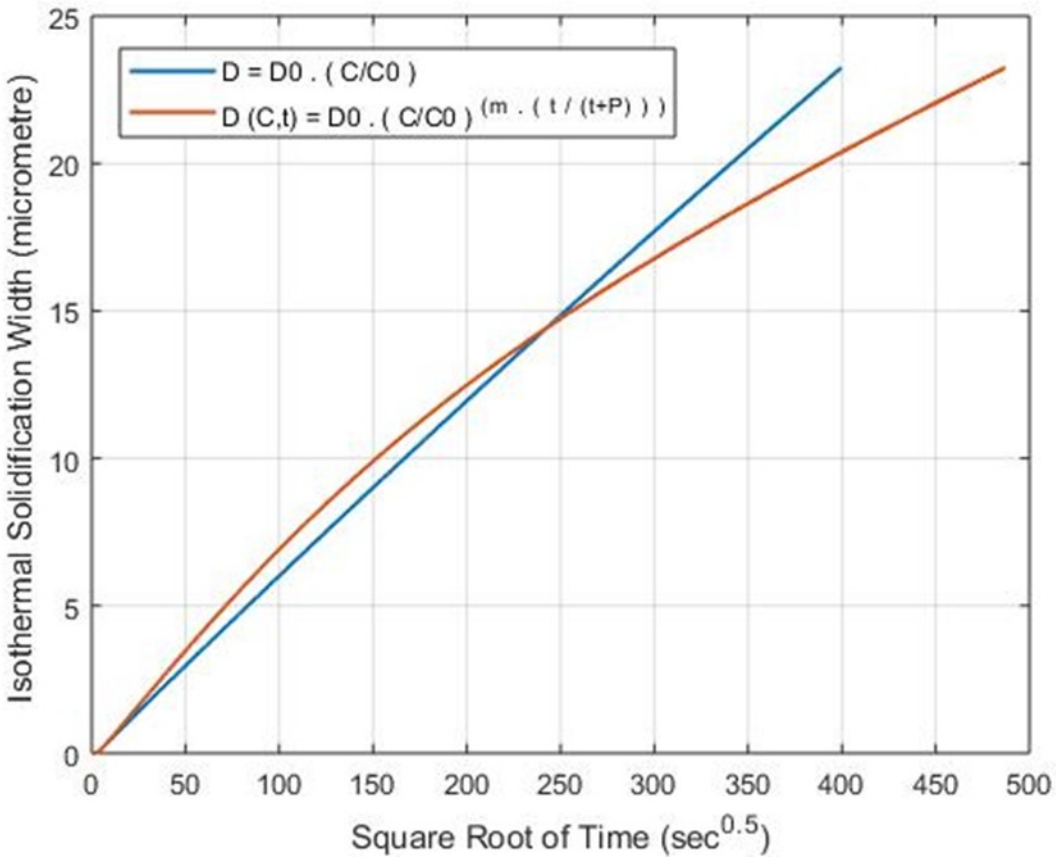

Figure 32: Illustration of the effect of concentration and time-dependent diffusion coefficient (Equation 38) on the extent of the deviation from parabolic behavior for the process in a cylindrical system.

4.3. Numerical Simulation of Homogenization Stage of TLP Bonding

After complete isothermal solidification, another crucial issue that can affect the properties of TLP bonded materials is the solute concentration at the center of the joint (C_s). It is often desirable that C_s should reduce below a certain level to avoid degradation in material properties. Therefore, post isothermal solidification heat treatment, often called homogenization is usually performed to reduce C_s to an acceptable value. The reduction in C_s is fundamentally controlled by further solute diffusion inside the substrate material. Therefore, during homogenization, two factors are very important: 1) Solute penetration inside the substrate, 2) C_s reduction. The kinetics of these two events after complete isothermal solidification are crucial. In this section, the new model developed in this research is used to study the kinetics of solute penetration and C_s reduction under two conditions in planar and non-planar interface systems: 1) constant diffusivity and 2) variable diffusion coefficient.

4.3.1. Solute Penetration and Surface Concentration Reduction Kinetics during the Homogenization Process with Constant Diffusivity

Variations in the depth of solute penetration (H_p) with $\sqrt{t}$ during the homogenization process in planar, cylindrical, and spherical systems, when *D* is constant, are presented in Figure 33. It is seen that H_p (Figure 34) varies linearly with $\sqrt{t}$ in all the systems. To compare this homogenization behavior to what occurs during isothermal solidification, under the same condition, depth of isothermal solidification solute penetration (IS_p) against $\sqrt{t}$ is plotted in Figure 35 (when the diffusion direction is along the direction of decrease in the radius of curvature). It can be observed that although IS_p (Figure 36) varies linearly with $\sqrt{t}$ only in the planar system during isothermal solidification, H_p has a linear relationship with $\sqrt{t}$ in all systems during the homogenization process.

Figure 37 shows how surface concentration (C_s) changes with $\sqrt{t}$ during the homogenization process in planar, cylindrical and spherical systems. It can be seen that during the process with constant diffusivity $1/C_s$ does not follow a linear relationship with $\sqrt{t}$ in non-planar (spherical and cylindrical) systems. It is, however, found in this work that, when *D* is constant, $1/C_s$ varies linearly with $\sqrt[2/g]{t}$, where g is a geometry factor, which is 1, 2 and 3 for planar, cylindrical and spherical systems, respectively. Therefore, when *D* is constant, it is possible to represent the kinetics of C_s reduction during homogenization in planar, cylindrical and spherical systems by a constant parameter, μ, the slope of the linear plot of $1/C_s$ against $\sqrt[2/g]{t}$. This finding has not been previously reported in the literature.

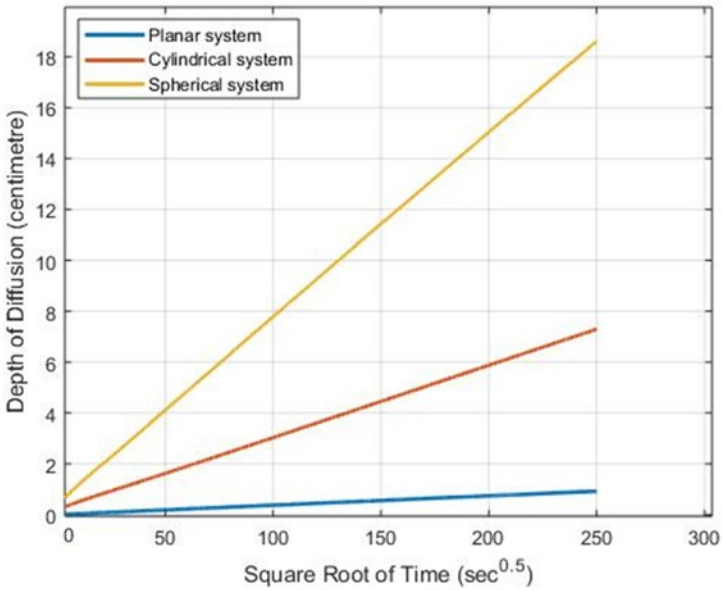

Figure 33: Variation of the depth of solute penetration with $\sqrt{t}$ for homogenization with constant diffusion coefficient in planar, cylindrical and spherical interface systems.

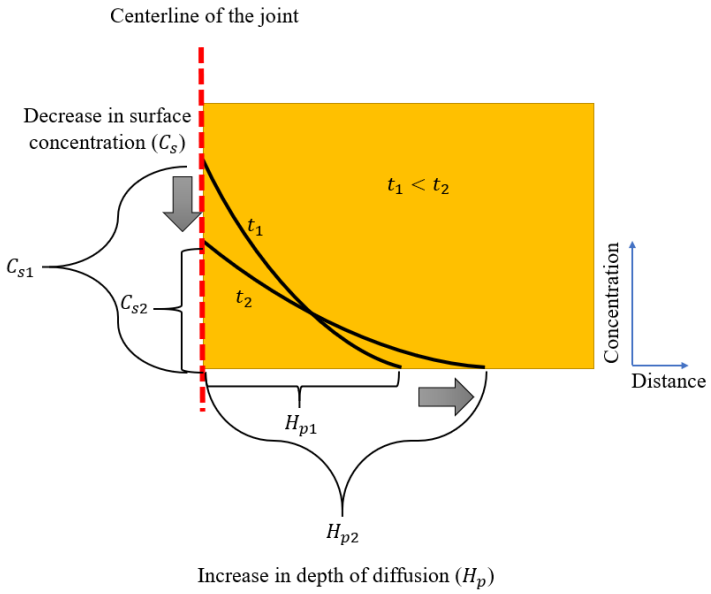

Figure 34: Schematic illustration of increase in depth of diffusion (H_p) and decrease in surface concentration (C_s) during the homogenization process.

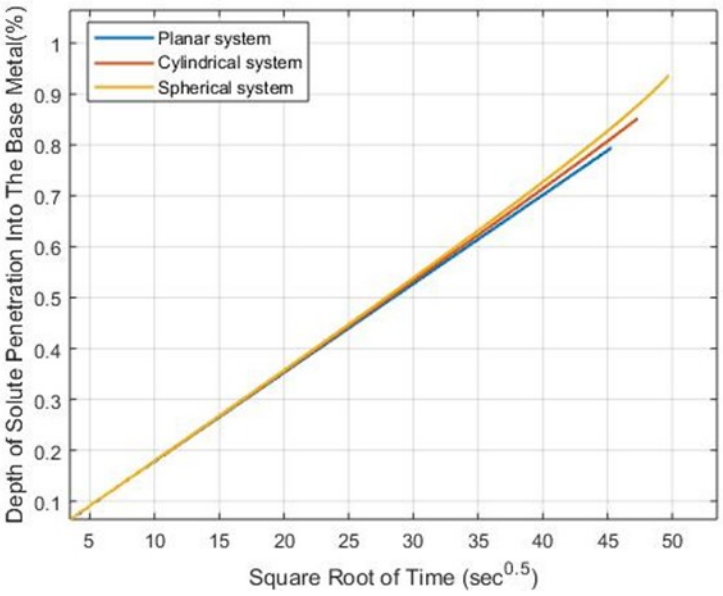

Figure 35: Variation of the depth of solute penetration with $\sqrt{t}$ for isothermal solidification with constant diffusion coefficient in planar, cylindrical and spherical interface systems.

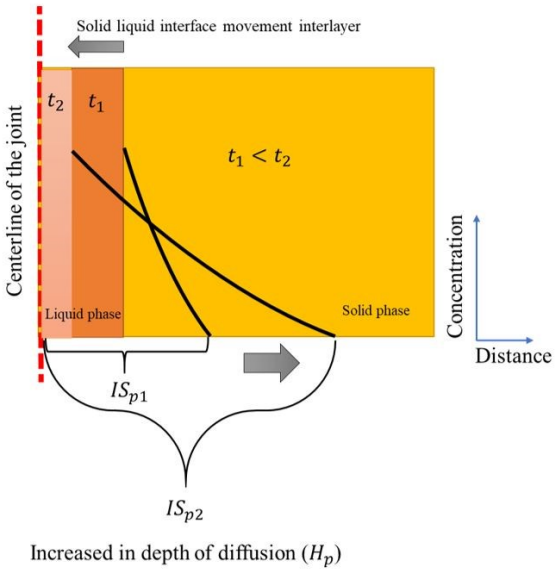

Figure 36: Schematic illustration of increase in depth of diffusion (IS_p) and decrease in surface concentration (C_s) during the homogenization process.

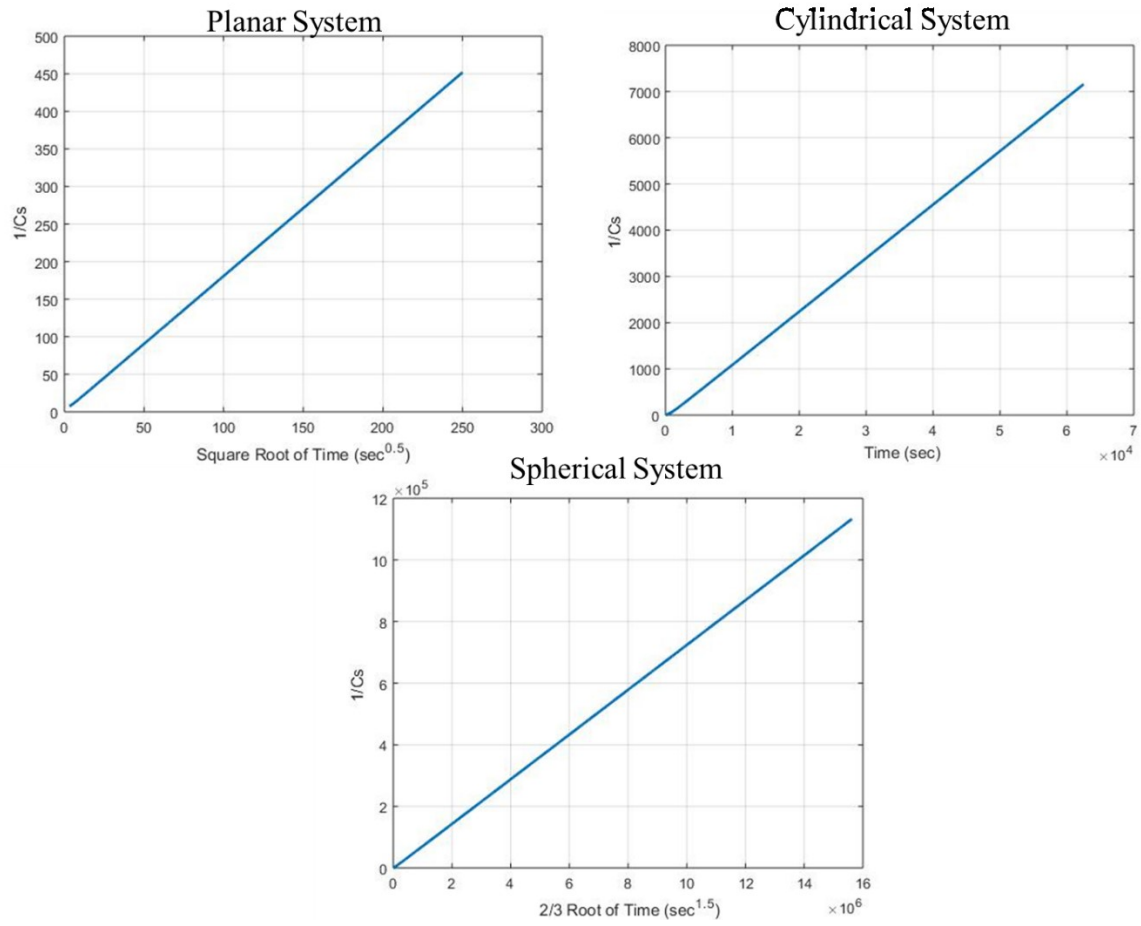

Figure 37: Illustration of a linear relationship between $\frac{1}{C_s}$ and $\sqrt[2/g]{t}$ for homogenization with a constant diffusivity, in which g is a geometry factor that can be 1, 2, and 3 for planar, cylindrical, and spherical systems respectively.

4.3.2. Solute Penetration and Surface Concentration Reduction Kinetics during Homogenization Process with Concentration-Dependent Diffusivity

To study the effect of concentration-dependent diffusivity on homogenization kinetics, power law concentration dependency of D (Equation 21) is used as a case of study. Figure 38 shows how the depth of solute penetration (H_p) changes with $\sqrt{t}$ after complete isothermal solidification in the planar system, when diffusivity depends on concentration through the power law function (Equation 21). It can be seen that during the homogenization process where D varies with concentration, in a planar system, the kinetics of the solute penetration cannot be represented by a rate constant parameter. To compare this homogenization kinetics behavior to what occurs during isothermal solidification, depth of solute penetration (IS_p) against $\sqrt{t}$ during the isothermal solidification with concentration dependent diffusivity is plotted in Figure 39. It can be observed that during isothermal solidification with concentration dependent diffusivity, in a planar system, the solute penetration kinetics can indeed be represented by a constant rate parameter, μ, the slope of the linear plot. This is in contrast to the kinetics of solute penetration during the homogenization process. Nevertheless, it is found that during homogenization in a planar system when D has a power law dependency on concentration (Equation 21), H_p has a linear relationship with $\sqrt[m+2]{t}$ during homogenization. In such a situation, the process kinetics can be represented by a constant rate parameter, if H_p is plotted against $\sqrt[m+2]{t}$.

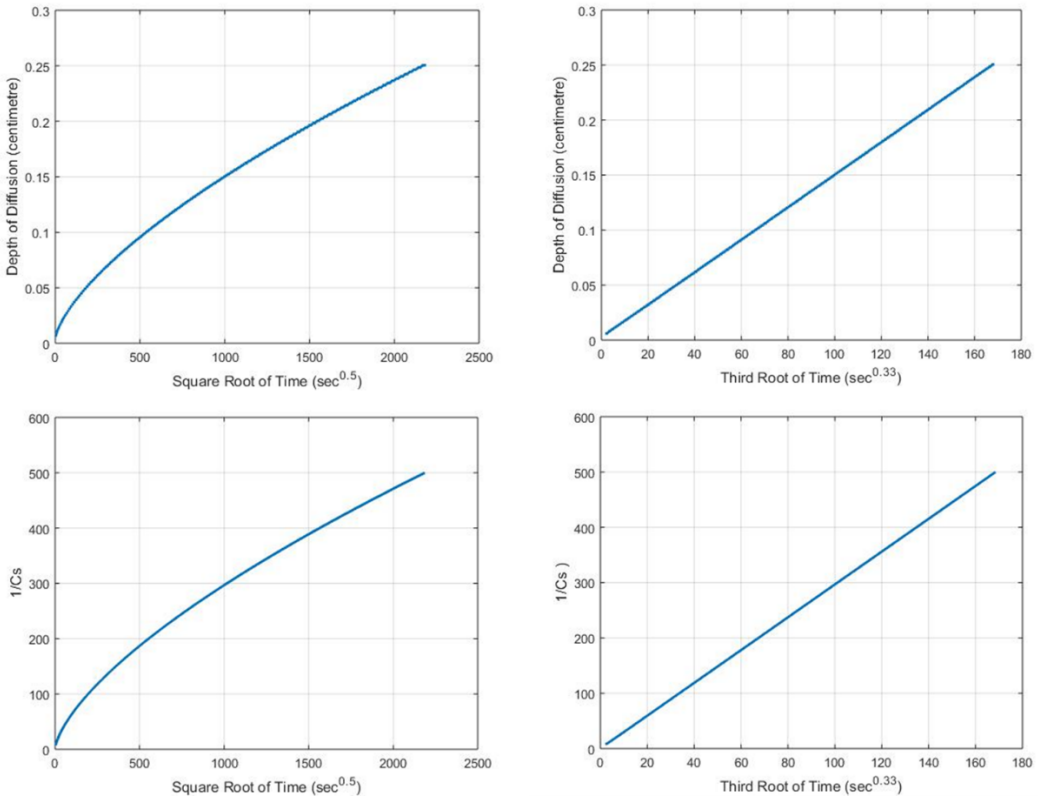

Figure 38: Illustration of the kinetics of solute penetration and C_s reduction during homogenization in a planar system with a power-law $D_{(c)}$ (with exponent $m = 1$).

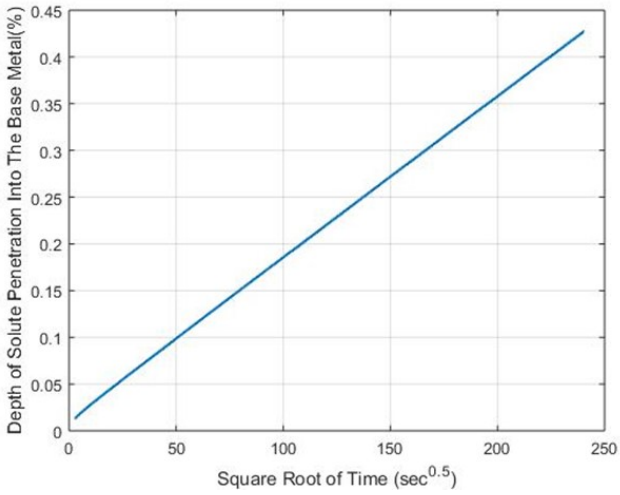

Figure 39: Variation of the solute penetration with $\sqrt{t}$ during isothermal solidification with a power-law $D_{(c)}$ (with exponent $m = 1$) in a planar system.

Figure 40 shows how the depth of solute penetration (H_p) varies with $\sqrt{t}$ during homogenization with $D_{(c)}$ based on the power law function (Equation 21) in a non-planar system (a cylindrical system is selected as an example). It can be seen from Figure 40 that, similar to the case in the planar system, the relationship between H_p and $\sqrt{t}$ in non-planar systems is non-linear but the extent of the non-linearity is greater in the non-planar systems compared to the planar system. In general, for the case of power law concentration dependent diffusivity (Equation 21), H_p follows a linear relationship with $\sqrt[(g.m+2)]{t}$, where g is the geometry factor with values of 1, 2 and, 3 for planar, cylindrical, and spherical interface systems, respectively. All the deviations from the linear behavior during homogenization are primary due to the fact that the maximum solute concentration in the solid, C_s, reduces with time. In contrast, during isothermal solidification, the maximum solute concentration in the solid, $C_{\alpha L}$, is constant and does not change with time.

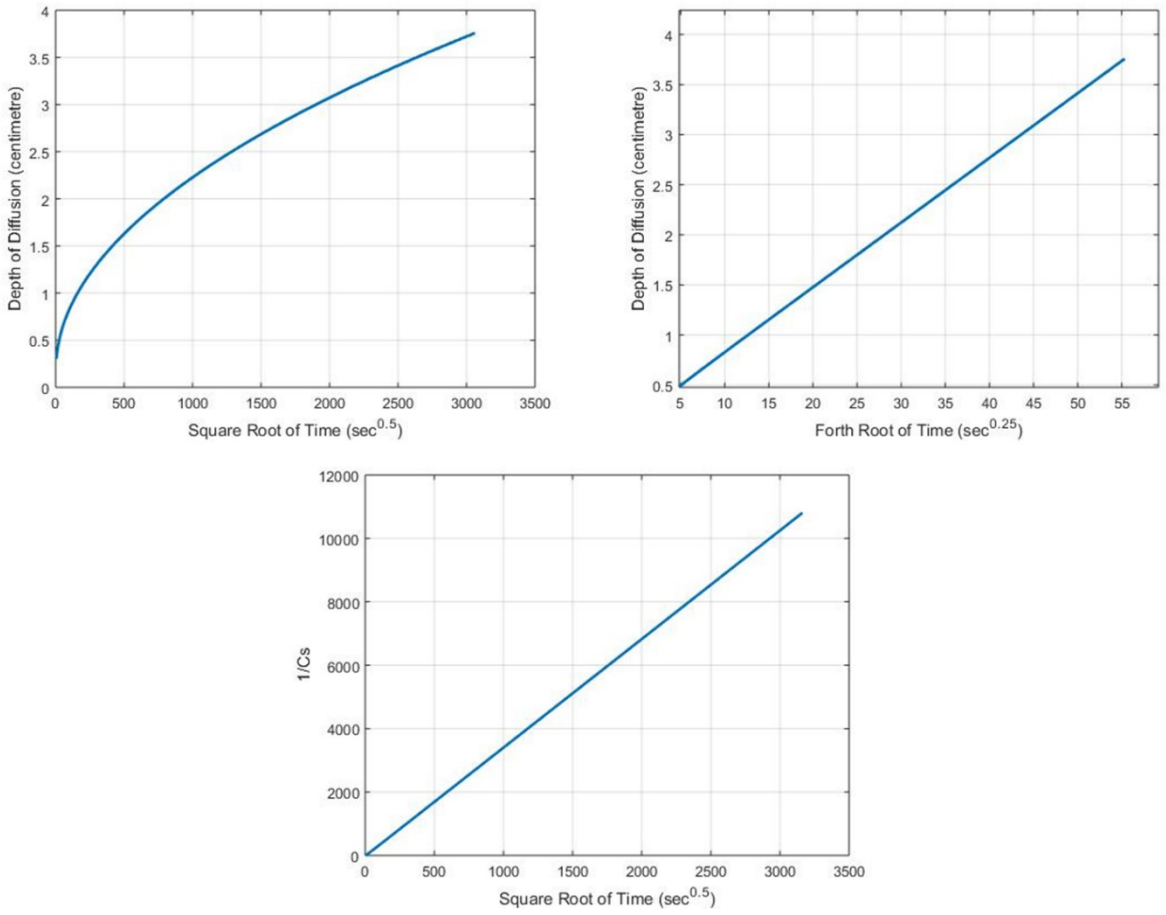

Figure 40: Illustration of the kinetics of solute penetration and C_s reduction during homogenization with the power law $D_{(c)}$ (exponent $m = 1$) in a cylindrical system.

Figure 38 shows how $\frac{1}{C_s}$ varies with $\sqrt{t}$ during the homogenization process for the case where *D* varies with concentration based on the power function (Equation 21) in a planar system. It can be seen from the Figure 38 that $\frac{1}{C_s}$ does not change linearly with $\sqrt{t}$, which is in contrast to the case when D is constant. Therefore, the kinetics of C_s reduction cannot be represented by a constant rate parameter when the diffusivity is a function of concentration in a planar system. The is generally the same case in the non-planar systems. It is, however, found that during homogenization with the power law $D_{(c)}$ (Equation 21), $\frac{1}{C_s}$ has a linear relationship with $\sqrt[(g.m+2)/g]{t}$, where the values of g are 1, 2, and 3 for planar, cylindrical, and spherical systems, respectively. As an example, when the power law exponent $m = 1$ in a cylindrical system, $\frac{1}{C_s}$ has a linear relationship with $\sqrt{t}$ as shown in Figure 40. No experimental data on TLP bonding homogenization kinetics are found in the literature to verify the theoretical findings in this research. However, experimental study of diffusion in semi-conductors where diffusivity varies with concentration based on the power law function in Equation 21 and exponent $m = 1$, with the similar initial and boundary conditions to those used in this present work exists [41]. The experimental results show that when the maximum solute concentration in the solid, C_s changes with time, in a planar system, solute penetration and $\frac{1}{C_s}$ has a linear relationship with third-root of time [41], which concurs with the predictions by the new numerical model developed in this research. It should, however, be noted that if $D_{(c)}$ is not in the power law form (Equation 21) or changes with time, H_p and $\frac{1}{C_s}$ will have relationships with holding time different from those reported for the power law function in the thesis.

Chapter 5: Summary and Conclusions

The objective of the present study is to develop a new TLP numerical model and use the model to study the effect of variable diffusivity on the kinetics of isothermal solidification and homogenization processes during TLP bonding in planar, cylindrical and spherical systems. The key findings are summarized as follows:

1- The dependency of the diffusion coefficient on concentration can profoundly affect the kinetics of isothermal solidification. Notwithstanding the variation of D with concentration, the kinetics of the isothermal solidification process with concentration-dependent diffusivity ($D_{(C)}$) can be represented by constant parameter $\emptyset$, known as the isothermal rate constant.

2- In comparison with the case where diffusivity is constant, when D increases with increases in concentration, $\emptyset$ reduces, while $\emptyset$ increases in cases where D decreases with increases in concentration. In the case where D fluctuates with increase in concentration, change in $\emptyset$ depends on whether the average value of D over the whole concentration range is higher or lower than that of the case where D is constant.

3- In the very rarely reported case where the concentration dependency of D varies with time, the kinetics of the isothermal solidification process cannot be represented by a constant parameter, since deviation from the linear relationship between the extent of isothermal solidification and $\sqrt{t}$ occurs. This key finding, which is confirmed by previously reported experimental data, constitutes a new explanation for the occurrence of deviation from the parabolic law behavior and it can explicate the deviation occurrence in systems where prior suggested reasons in the literature do not apply.

4- If the function through which D varies with concentration changes with temperature, it is possible for an increase in temperature to produce a reduction in the kinetics of isothermal solidification, which is in contrast to most of the cases reported in the literature, where the kinetics increase with temperature.

5- Aside from time-dependent diffusivity, non-planar solid-liquid interface, specifically, cylindrical and spherical shapes, is another factor that causes deviation from the parabolic law even when D is constant.

6- The geometry-induced deviation can either be positive or negative depending on the location of the liquid relative to the curvature of the interface. This is at variance to what occurs in the planar interface system, where the liquid location relative to the solid-liquid interface does not alter the kinetics of isothermal solidification process.

7- In cylindrical and spherical systems, when the solute diffusion direction is opposite to the direction of increase in the radius of interface curvature, the size of the substrate can influence isothermal solidification kinetics, even when the solute does not reach the center of the substrate. In the planar system, however, the size of the substrate does not affect the kinetics of the isothermal solidification.

8- The kinetics of diffusion-controlled solute penetration during the homogenization stage that follows isothermal solidification is found to be significantly different from the kinetics of solute penetration during the isothermal solidification stage.

9- Although there is deviation from the linear relationship between the depth of solute penetration and $\sqrt{t}$ when D is constant during the isothermal solidification in non-planar systems, there is no such deviation when D is constant during homogenization in planar and non-planar (cylindrical and spherical) systems.

10- In a planar system where diffusivity is dependent on concentration, the depth of solute penetration follows a linear relationship with $\sqrt{t}$ during isothermal solidification, in contrast, however, under a similar condition, the solute penetration deviates from the linear relationship with $\sqrt{t}$ during homogenization. The differences between the kinetics of isothermal solidification and homogenization stages are fundamentally attributable to the fact that while the maximum solute concentration in the solid during homogenization changes with time, it does not vary with time during the isothermal solidification process.

Chapter 6: Suggestions for Future Work

The present numerical TLP bonding model is used to study the effect of variable diffusion coefficients on the isothermal solidification and homogenization kinetics in planar and non-planar (cylindrical and spherical) systems, where a single diffusing element is involved. However, to investigate the TLP bonding kinetics further, the following points are recommended:

1- Further study should be performed to investigate how the presence of multiple MPD solutes in a multi-component filler alloy would affect the kinetics of isothermal solidification and homogenization when the diffusivities of the solutes change with concentration and time.

2- The numerical model developed in this work can be extended to study cases where a temperature gradient is imposed on the materials being bonded and investigate how the kinetics of the isothermal solidification and homogenization stages are affected by variable diffusivity under an imposed temperature gradient.

Appendix: Formulations and Algorithms of the Model

TLP bonding is a system of partial differential equations for distinct phases with a moving boundary problem. Calculation of the interface position movement and adjusting the new calculated location to the new coordinate system with time is one of the most challenging aspects of the TLP bonding numerical simulation. As previously discussed, the diffusion coefficient in the solid phase is not constant during the TLP bonding process. Hence, for the TLP bonding solutions with variable diffusivity, power law concentration-dependent diffusion coefficient (Equation 21) is selected as an example. However, this approach can be applied for any function of the diffusion coefficient. Based on the Landau transformation method [24], a as a local distance transformation equation in the liquid phase A can be defined as follows:

$$a = \frac{x}{s(t)} \quad , \quad 0 < a < 1 \quad , \quad 0 < x < s(t) \qquad \text{Equation A.1}$$

Where x is the distance from the main coordinate and $\mathrm{s(t)}$ is the position of the interface at the time (t). Based on Equation A.1, x is between 0 and $\mathrm{s(t)}$, which makes the value of a (normalized distance in the liquid phase A) to be between 0 and 1. Therefore it can be represented that:

$$\frac{\partial a}{\partial x} = \frac{1}{s(t)} \qquad \text{Equation A.2}$$

$$\frac{\partial^2 a}{\partial x^2} = \frac{1}{s(t)^2} \qquad \text{Equation A.3}$$

$$\frac{\partial a}{\partial t} = \frac{0 \times (s_{(t)}) - (s_{(t)}'(x))}{(s_{(t)})^2} = \frac{-(s_{(t)}'(x))}{(s_{(t)})^2} \qquad \text{Equation A.4}$$

$$\frac{\partial C_a(x,t)}{\partial x} = \frac{\partial a}{\partial x} \times \frac{\partial C_a(a,t)}{\partial a} = \frac{1}{s(t)} \times \frac{\partial C_a(a,t)}{\partial a} \qquad \text{Equation A.5}$$

$$\frac{\partial^2 C_a(x,t)}{\partial x^2} = \frac{\partial^2 a}{\partial x^2} \times \frac{\partial^2 C_a(a,t)}{\partial a^2} = \frac{1}{s(t)^2} \times \frac{\partial^2 C_a(a,t)}{\partial a^2}$$ Equation A.6

$$\frac{\partial C_a(x,t)}{\partial t} = \frac{\partial a}{\partial t} \times \frac{\partial C_a(a,t)}{\partial a} + \frac{\partial C_a(a,t)}{\partial t} = \frac{-(s_{(t)}{}'(x))}{(s_{(t)})^2} \times \frac{\partial C_a(a,t)}{\partial a} + \frac{\partial C_a(a,t)}{\partial t}$$ Equation A.7

Where $C_a(x,t)$ is the concentration in the liquid phase A as a function of distance x and time t and $C_a(a,t)$ is the concentration in the liquid phase A as a function of normalized distance a and time t. Therefore, by applying Equations A.2 to A.7, it can be possible to rewrite Fick's second law equation with a constant diffusion coefficient in the normalized form as follows:

$$-a \times \frac{ds}{dt} \times \frac{\partial C_a(a,t)}{\partial a} + s_{(t)} \times \frac{\partial C_a(a,t)}{\partial t} = \frac{D}{s_{(t)}} \times \frac{\partial^2 C_a(a,t)}{\partial a^2}$$ Equation A.8

The normalized form of Fick's second law can be more precise by applying the following Equations:

$$\frac{\partial (C_a \times a)}{\partial a} = C_a + a \frac{\partial C_a}{\partial a}$$ Equation A.9

$$\frac{\partial (C_a \times s)}{\partial t} = C_a \frac{ds}{dt} + s \frac{\partial C_a}{\partial t}$$ Equation A.10

Therefore, the transformed diffusion equation for the liquid phase A, with a constant diffusion coefficient can be shown as follows:

$$\frac{\partial (C_a s)}{\partial t} = \frac{ds}{dt} \times \frac{\partial (C_a a)}{\partial u} + \frac{D}{s_{(t)}} \times \frac{\partial^2 C_a(a,t)}{\partial a^2}$$ Equation A.11

For solving Equation A.11 with respect to distance and time, a fully-implicit solution of concentration distribution in the liquid phase A can be illustrated as follows [5]:

$$\left(s^f\left(C_{a_i}{}^f\right) - s^c\left(C_{a_i}{}^c\right)\right) \times (\Delta a) = (s^f - s^c) \times \left(C_{a_{i+1/2}}{}^f a_{i+1/2} - C_{a_{i-1/2}}{}^f a_{i-1/2}\right) +$$

$$D_A\left(\frac{\Delta t}{\Delta a \times s^f}\left(C_{a_{i+1}}{}^f - 2C_{a_i}{}^f + C_{a_{i-1}}{}^f\right)\right)$$ Equation A.12

Where superscripts c and f correspond to the current time step and one time step ahead respectively, subscript i shows the node number, which is considered for analysis in the algorithm and $i-1$ and $i+1$ are nodes before and after the node i respectively. In addition, $i+\frac{1}{2}$ is the node between nodes i and $i+1$ and $i-\frac{1}{2}$ is the node between nodes $i-1$ and i. s^c and s^f show the positions of the interface at the current time step and one time step ahead respectively. $C_{a_i}{}^c$ and $C_{a_i}{}^f$ are the current and future concentration (the future concentrations are unknown factors in the system) at node i in the liquid phase respectively. The position of the nodes in local coordinate can be shown as a, which $a_{i+1/2}$ is the local position in the liquid phase between grid points i and $i+1$ and $a_{i-1/2}$ is the local position in the liquid phase between grid points i and $i-1$. In addition, Δa is the distance between 2 nodes in the liquid phase. Δt is the time step and D_A is the constant diffusion coefficient in the liquid phase. However, Equation A.12 can be rewritten as follows:

$$-(A)C_{a_{i-1}}{}^f + (B)C_{a_i}{}^f - (C)C_{a_{i+1}}{}^f = D$$ Equation A.13

Future concentrations in Equation A.13 are unknown values, which can be calculated by the tri-diagonal matrix method. When the interface velocity is positive, the known factors A, B, C and D are as follows:

$$A = \frac{D_A \Delta t}{\Delta a \times s^f}$$ Equation A.14

$$B = s^f \Delta a + (s^f - s^c)\frac{a_i + a_{i-1}}{2} + \frac{2D_A \Delta t}{\Delta a \times s^f}$$ Equation A.15

$$C = (s^f - s^c)\frac{a_i + a_{i+1}}{2} + \frac{D_A\,\Delta t}{\Delta a \times s^f}$$ Equation A.16

$$D = \Delta a\; s^c C_{a_i}^{\mathrm{c}}$$ Equation A.17

However, if the velocity is negative the known factors A, B, C, and D can be calculated as follows:

$$A = -(s^f - s^c)\frac{a_i + a_{i-1}}{2} + \frac{D_A\,\Delta t}{\Delta a \times s^f}$$ Equation A.18

$$B = s^f \Delta a - (s^f - s^c)\frac{a_{i+1} + a_i}{2} + \frac{2D_A\,\Delta t}{\Delta a \times s^f}$$ Equation A.19

$$C = \frac{D_A\,\Delta t}{\Delta a \times s^f}$$ Equation A.20

$$D = \Delta a\; s^c C_{a_i}^{\mathrm{c}}$$ Equation A.21

The unknown values of future concentrations at each time step can be calculated by the tri-diagonal matrix as follows:

$$K_1 = \frac{C_1}{B_1}$$, First node $i = 1$ Equation A.22

$$O_1 = \frac{D_1}{B_1}$$, First node $i = 1$ Equation A.23

$$K_i = \frac{C_i}{B_i - A_i \times K_{i-1}}$$, Node i Equation A.24

$$O_i = \frac{D_i + A_i \times O_{i-1}}{B_i - A_i \times K_{i-1}}$$, Node i Equation A.25

$$O_n = \frac{D_n + A_n \times O_{n-1}}{B_n - A_n \times K_{n-1}}$$, Last node $i = n$ Equation A.26

$$C_{a_{\mathrm{n}}}^{\mathrm{f}} = O_n$$ Equation A.27

$$C_{a_i}^{f} = O_i + K_i \times C_{a_{i+1}}^{f}$$ Equation A.28

Landau transformation method [24] can be applied for the solid phase B, where distance transformation equation b can be defined as follows:

$$b = \frac{x - s(t)}{L - s(t)} \quad , \quad 0 < b < 1 \quad , \quad s(t) < x < L$$ Equation A.29

Where x is the distance between $s(t)$ and L, which makes the value of b (normalized distance in the solid phase B) to be between 0 and 1. Therefore, it can be represented that:

$$\frac{\partial b}{\partial x} = \frac{1}{L - s(t)}$$ Equation A.30

$$\frac{\partial^2 b}{\partial x^2} = \frac{1}{(L - s(t))^2}$$ Equation A.31

$$\frac{\partial b}{\partial t} = \frac{-s_{(t)}'(L - s_{(t)}) - (-s_{(t)}'(x - s_{(t)})}{(L - s_{(t)})^2} \Longrightarrow \frac{x - s_{(t)} - (L - s_{(t)})}{(L - s_{(t)})^2} s_{(t)}' = \frac{b-1}{L - s_{(t)}} s_{(t)}'$$ Equation A.32

$$\frac{\partial C_b(x,t)}{\partial x} = \frac{\partial b}{\partial x} \times \frac{\partial C_b(b,t)}{\partial b} = \frac{1}{L - s(t)} \times \frac{\partial C_b(b,t)}{\partial b}$$ Equation A.33

$$\frac{\partial^2 C_b(x,t)}{\partial x^2} = \frac{\partial^2 b}{\partial x^2} \times \frac{\partial^2 C_b(b,t)}{\partial b^2} = \frac{1}{(L - s(t))^2} \times \frac{\partial^2 C_b(b,t)}{\partial b^2}$$ Equation A.34

$$\frac{\partial C_b(x,t)}{\partial t} = \frac{\partial b}{\partial t} \times \frac{\partial q(b,t)}{\partial b} + \frac{\partial q(b,t)}{\partial t} = \frac{b-1}{L - s_{(t)}} \times \frac{ds}{dt} \times \frac{\partial C_b(b,t)}{\partial b} + \frac{\partial C_b(b,t)}{\partial t}$$ Equation A.35

By combining Equations A.30 to A.35 with diffusion equation, transformed diffusion equation to the local coordination for the solid phase B can be illustrated as follows:

$$(b-1) \times \frac{ds}{dt} \times \frac{\partial C_b(b,t)}{\partial b} + \big(L - s(t)\big) \times \frac{\partial C_b(b,t)}{\partial t} = \frac{\left(\frac{D_0}{C_0^{\,m}}\right)}{\big(L - s(t)\big)} \left(\frac{\partial}{\partial b}\left(C_b(b,t)^m \frac{\partial C_{b(b,t)}}{\partial b}\right)\right)$$ Equation A.36

Equation A.36 can be more precise by applying the following equations:

$$\frac{\partial(C_b(1-b))}{\partial b} = -C_b(b,t) + (1-b)\frac{\partial C_b}{\partial b} \quad \text{Equation A.37}$$

$$\frac{\partial(C_b(L-s))}{\partial t} = -C_b\frac{ds}{dt} + (L-s)\frac{\partial C_b}{\partial t} \quad \text{Equation A.38}$$

Therefore, the transformed diffusion equation for the solid phase B, with a diffusion coefficient as a power function of concentration in the solid phase can be shown as follows:

$$\frac{\partial(C_b(L-s))}{\partial t} = \frac{ds}{dt} \times \frac{\partial(C_b(1-b))}{\partial b} + \frac{\left(\frac{D_0}{{C_0}^m}\right)}{(L-s(t))}\left(\frac{\partial}{\partial b}\left({C_b}^m \frac{\partial C_{b(b,t)}}{\partial b}\right)\right. \quad \text{Equation A.39}$$

The integral of nonlinear Equation A.39 with respect to the distance and time can be solved by an explicit method to calculate concentration distribution in the solid phase B as the following equation:

$$\left({C_b}_i^f(L-s^f) - {C_b}_i^c(L-s^c)\right)\Delta b = (s^f - s^c) \times \left({C_b}_{i+\frac{1}{2}}^c\left(1-b_{i+1/2}\right) - {C_b}_{i-\frac{1}{2}}^c\left(1-b_{i-1/2}\right)\right) +$$

$$\frac{\left(\frac{D_0}{{C_0}^m}\right).\Delta t}{(L-s^c)\Delta b}\left(\left({C_b}_{i+\frac{1}{2}}^{c\ m}\right)\left({C_b}_{i+1}^c - {C_b}_i^c\right) - \left({C_b}_{i-\frac{1}{2}}^{c\ m}\right)\left({C_b}_i^c - {C_b}_{i-1}^c\right)\right) \quad \text{Equation A.40}$$

Where ${C_b}_i^c$ and ${C_b}_i^f$ are the current and future solute concentrations at the node i in the solid phase B. The position of nodes in local coordinate for the solid phase is shown as b, which $b_{i+1/2}$ is the local position in the solid phase between grid points i and $i+1$ and $b_{i-1/2}$ is the local position in the solid phase between grid point i and $i-1$. Also, Δb is the distance between 2 nodes in the solid phase B, and L is the width of base metal plus half-width of filler alloy in the system.

Landau transformation method [24] can be used for non-planar geometries to calculate the diffusion equation. If the diffusion direction is along the increase radius of curvature, phase A is liquid, and phase B is solid in the present numerical solution. Therefore, concentration distribution in the liquid phase A by an implicit method can be shown as follows:

$$\Delta a(C_{a_i}^{f} s^f((s^f a_i)^g) - C_{a_i}^{c} s^c((s^c a_i)^g)) = \Delta t(\ \left(s^f\left(a_{i+1/2}\right)\right)^g \left(\frac{s^f - s^c}{\Delta t} C_{a_{i+1/2}}^{f} a_{i+1/2} + \frac{D_A}{s^f}\frac{\left(C_{a_{i+1}}^{f} - C_{a_i}^{f}\right)}{\Delta u}\right) - \left(s^f a_{i-1/2}\right)^g \left(\frac{s^f - s^c}{\Delta t} C_{a_{i-1/2}}^{f} a_{i-1/2} + \frac{D_A}{s^f}\frac{\left(C_{a_i}^{f} - C_{a_{i-1}}^{f}\right)}{\Delta u}\right)\ \ ) \qquad \text{Equation A.41}$$

Where g is the geometry factor that can be 1 and 2 for cylindrical and spherical systems respectively. Future concentrations as unknown values that can be calculated by tri-diagonal matrix method. When the interface velocity is positive, the known factors A, B, C, and D are as follows:

$$A = \frac{D_A(\ s^f\left(\frac{a_i + a_{i-1}}{2}\right))^g\ \Delta t}{\Delta a \times s^f} \qquad \text{Equation A.42}$$

$$B = s^f \Delta a (s^f a_i)^g + (s^f - s^c)\left(\ s^f\left(\frac{a_i + a_{i-1}}{2}\right)\right)^g \left(\frac{a_i + a_{i-1}}{2}\right) + \frac{D_A\ (\ s^f\left(\frac{a_i + a_{i+1}}{2}\right))^g \Delta t}{\Delta a \times s^f} + \frac{D_A\ (\ s^f\left(\frac{a_i + a_{i-1}}{2}\right))^g \Delta t}{\Delta a \times s^f} \qquad \text{Equation A.43}$$

$$C = (s^f - s^c)\left(\ s^f\left(\frac{a_i + a_{i+1}}{2}\right)\right)^g \left(\frac{a_i + a_{i+1}}{2}\right) + \frac{D_A(\ s^f\left(\frac{a_i + a_{i+1}}{2}\right))^g\ \Delta t}{\Delta a \times s^f} \qquad \text{Equation A.44}$$

$$D = \Delta a\ s^c C_{a_i}^{c}(\ s^c(a_i)\ )^g \qquad \text{Equation A.45}$$

However, if the velocity is negative the known factors A, B, C, and D are as follows:

$$A = \frac{D_A(\ s^f\left(\frac{a_i + a_{i-1}}{2}\right))^g\ \Delta t}{\Delta a \times s^f} - (s^f - s^c)\left(\ s^f\left(\frac{a_i + a_{i-1}}{2}\right)\right)^g \left(\frac{a_i + a_{i-1}}{2}\right) \qquad \text{Equation A.46}$$

$$B = s^f \Delta a (s^f a_i)^g + (s^f - s^c)\left(s^f \left(\frac{a_i + a_{i+1}}{2}\right)\right)^g \left(\frac{a_i + a_{i+1}}{2}\right) + \frac{D_A \left(s^f \left(\frac{a_i + a_{i+1}}{2}\right)\right)^g \Delta t}{\Delta a \times s^f} +$$

$$\frac{D_A \left(s^f \left(\frac{a_i + a_{i-1}}{2}\right)\right)^g \Delta t}{\Delta a \times s^f} \qquad \text{Equation A.47}$$

$$C = \frac{D_A \left(s^f \left(\frac{a_i + a_{i+1}}{2}\right)\right)^g \Delta t}{\Delta a \times s^f} \qquad \text{Equation A.48}$$

$$D = \Delta a \; s^c C_{a_i}^{c} \left(s^c (a_i) \right)^g \qquad \text{Equation A.49}$$

By tri-diagonal matrix method (Equations A.22 to A.28), the concentration of each grid point at each time step can be calculated for the liquid phase A. The diffusion coefficient in the solid phase is considered as a power form of concentration-dependent diffusion coefficient. However, concentration distribution in the solid phase B for non-planar interface systems by an explicit method can be shown as follows:

$$\Delta b \left[C_{b_i}^{f} (R - s^f)(b_i (R - s^f) + s^f)^g - C_{b_i}^{c} (R - s^c)(b_i (R - s^c) + s^c)^g \right] = \Delta t \left(\left((R - s^c) b_{i+\frac{1}{2}} + s^c \right)^g \left(\frac{s^f - s^c}{\Delta t} C_{b_{i+\frac{1}{2}}}^{c} \left(1 - b_{i+\frac{1}{2}}\right) + \frac{\left(\frac{D_0}{C_0^m}\right) . C_{b_{i+1/2}}^{c}}{R - s^c} \frac{\left(C_{b_{i+1}}^{c} - C_{b_i}^{c}\right)}{\Delta b} \right) - \left((R - s^c) b_{i-\frac{1}{2}} + s^c \right)^g \left(\frac{s^f - s^c}{\Delta t} C_{b_{i-\frac{1}{2}}}^{c} \left(1 - b_{i-\frac{1}{2}}\right) + \frac{\left(\frac{D_0}{C_0^m}\right) . C_{b_{i-1/2}}^{c}}{R - s^c} \frac{\left(C_{b_i}^{c} - C_{b_{i-1}}^{c}\right)}{\Delta b} \right) \right) \qquad \text{Equation A.50}$$

In the condition, where the diffusion direction is along the decrease radius of curvature, diffusion equation in the solid phase A by the explicit method can be illustrated as the follows:

$$\Delta a\left(C_{a_i}^{\ f} s^f((s^f a_i)^g) - C_{a_i}^{\ c} s^c((s^c a_i)^g)\right) = \Delta t\left(\left(s^c a_{i+\frac{1}{2}}\right)^g \left(\frac{s^f - s^c}{\Delta t} C_{a_{i+\frac{1}{2}}}^{\ c} a_{i+\frac{1}{2}} + \frac{\left(\frac{D_0}{C_0^{\ m}}\right).\left(C_{a_{i+\frac{1}{2}}}^{\ c}{}^m\right)}{s^c} \frac{(C_{a_{i+1}}^{\ c} - C_{a_i}^{\ c})}{\Delta}\right) - \left(s^c a_{i-\frac{1}{2}}\right)^g \left(\frac{s^f - s^c}{\Delta t} C_{a_{i-\frac{1}{2}}}^{\ c} a_{i-\frac{1}{2}} + \frac{\left(\frac{D_0}{C_0^{\ m}}\right).\left(C_{a_{i-\frac{1}{2}}}^{\ c}{}^m\right)}{s^c} \frac{(C_{a_i}^{\ c} - C_{a_{i-1}}^{\ c})}{\Delta a}\right)\right)$$

Equation A.51

However, concentration distribution in the liquid phase B with a constant diffusion coefficient can be calculated by the Landau transformation method [24] as follows:

$$\Delta b\left[C_{b_i}^{\ f}(R - s^f)(b_i(R - s^f) + s^f)^g - C_{b_i}^{\ c}(R - s^c)(b_i(R - s^c) + s^c)^g\right] = \Delta t\left(\left((R - s^f)b_{i+\frac{1}{2}} + s^f\right)^g \left(\frac{s^f - s^c}{\Delta t} C_{b_{i+\frac{1}{2}}}^{\ f}\left(1 - b_{i+\frac{1}{2}}\right) + \frac{D_B}{R - s^f} \frac{\left(C_{b_{i+1}}^{\ f} - C_{b_i}^{\ f}\right)}{\Delta b}\right) - \left((R - s^f)b_{i-\frac{1}{2}} + s^f\right)^g \left(\frac{s^f - s^c}{\Delta t} C_{b_{i-\frac{1}{2}}}^{\ f}\left(1 - b_{i-\frac{1}{2}}\right) + \frac{D_B}{R - s^f} \frac{\left(C_{b_i}^{\ f} - C_{b_{i-1}}^{\ f}\right)}{\Delta b}\right)\right)$$

Equation A.52

Future concentrations as unknown values can be calculated by tri-diagonal matrix method. When the interface velocity is positive, the known factors A, B, C, and D are as follows:

$$A = \left((R - s^f)(\frac{b_i + b_{i-1}}{2}) + s^f\right)^g \frac{D_B \Delta t}{(R - s^f)\Delta b}$$

Equation A.53

$$B = \left((R - s^f)(b_i) + s^f\right)^g (R - s^f)\Delta b + \left((R - s^f)(\frac{b_{i+1} + b_i}{2}) + s^f\right)^g \frac{D_B \Delta t}{(R - s^f)\Delta b} + \left((R - s^f)(\frac{b_i + b_{i-1}}{2}) + s^f\right)^g \frac{D_B \Delta t}{(R - s^f)\Delta b} + \left((R - s^f)\left(\frac{b_i + b_{i-1}}{2}\right) + s^f\right)^g (R - s^f)(1 - \frac{b_i + b_{i-1}}{2})$$

Equation A.54

$$C = \left((R - s^f)(\frac{b_{i+1}+b_i}{2}) + s^f\right)^g \frac{D_B \Delta t}{(R-s^f)\Delta b} + \left((R - s^f)\left(\frac{b_{i+1}+b_i}{2}\right) + s^f\right)^g (R - s^f)(1 - \frac{b_{i+1}+b_i}{2})$$

Equation A.55

$$D = C_{b_i}^{\ c}(R - s^c)\Delta b(b_i(R - s^c) + s^c)^g$$ Equation A.56

However, if the velocity is negative the known factors A, B, C, and D are as follows:

$$A = \left((R - s^f)(\frac{b_i+b_{i-1}}{2}) + s^f\right)^g \frac{D_B \Delta t}{(R-s^f)\Delta b} - \left((R - s^f)\left(\frac{b_i+b_{i-1}}{2}\right) + s^f\right)^g (R - s^f)(1 - \frac{b_i+b_{i-1}}{2})$$

Equation A.57

$$B = \left((R - s^f)(b_i) + s^f\right)^g (R - s^f)\Delta b + \left((R - s^f)(\frac{b_{i+1}+b_i}{2}) + s^f\right)^g \frac{D_B \Delta t}{(R-s^f)\Delta b} + \left((R - s^f)(\frac{b_i+b_{i-1}}{2}) + s^f\right)^g \frac{D_B \Delta t}{(R-s^f)\Delta b} - \left((R - s^f)\left(\frac{b_{i+1}+b_i}{2}\right) + s^f\right)^g (R - s^f)(1 - \frac{b_{i+1}+b_i}{2})$$

Equation A.58

$$C = \left((R - s^f)(\frac{b_{i+1}+b_i}{2}) + s^f\right)^g \frac{D_B \Delta t}{(R-s^f)\Delta b}$$ Equation A.59

$$D = C_{b_i}^{\ c}(R - s^c)\Delta b(b_i(R - s^c) + s^c)^g$$ Equation A.60

Therefore, by using a tri-diagonal matrix (Equations A.22 to A.28), the concentration of each grid point at each time step in the liquid phase B can be calculated. All the equations above are applied to several grid nodes in both the liquid and solid phases at each time step to compute the solute concentration profiles. Thereafter, the calculated concentration profiles are used to predict the new position of the migrating solid-liquid interface for the next time step ahead. These calculation procedures are repeated until the isothermal solidification process is completed.

References

[1] W. D. Mucdonald and T. W. Eagar, “Transient Liquid Phase Bonding,” vol. 1, no. 1, pp. 23–46, 1992.

[2] and D. F. P. D.S. Duvall, W. A. Owczarski, “No Title,” *Weld. J.*, vol. 53, no. 203, p. 14, 1974.

[3] M. Abdelfattah, “An experimental and theoretical study of transient liquid phase bonding of nickel based materials,” 2008.

[4] W. D. MacDonald and T. W. Eagar, “Transient liquid phase bonding processes,” *Annu. Rev. Mater. Sci.*, vol. 1, no. 1, pp. 93–100, 1992.

[5] T. C. Illingworth, I. O. Golosnoy, V. Gergely, and T. W. Clyne, “Numerical modelling of transient liquid phase bonding and other diffusion controlled,” *Proc. Iv Int. Conf. Temp. Capillarity*, vol. 40, pp. 2505–2511, 2005.

[6] Y. Zhou and T. H. North, “Kinetic modelling of diffusion-controlled, two-phase moving interface problems,” *Model. Simul. Mater. Sci. Eng.*, vol. 1, no. 4, pp. 505–516, 1993.

[7] H. Nakagawa, C. H. Lee, and T. H. North, “Modeling of base metal dissolution behavior during transient liquid-phase brazing,” *Metall. Trans. A*, vol. 22, no. 2, pp. 543–555, 1991.

[8] S. R. Cain, J. R. Wilcox, and R. Venkatraman, “A diffusional model for transient liquid,” *Acta Mater.*, vol. 45, no. 2, pp. 701–707, 1997.

[9] N. Shinmura T., Ohsasa K., “Isothermal Solidification Behavior During the Transient Liquid Phase Bonding Process of Nickel Using Binary Filler Metals,” *Mater. Trans.*, vol. 42, no. 2, pp. 292–297, 2001.

[10] Tresa M. Pollock and Sammy Tin, “Nickel-Based Superalloys for Advanced Turbine Engines: Chemistry, Microstructure and Properties,” *J. Propuls. Power*, vol. 22, no. 2, pp. 361–374, 2006.

[11] M. K. Dinkel *et al.*, “New boron and silicon free single crystal-diffusion brazing alloys,” *Proc. Int. Symp. Superalloys*, pp. 211–220, 2008.

[12] G. R. A. Niemann J. T., “Transient Liquid Phase Bonding,” *Weld. J.*, vol. 52, no. 175, p. 184, 1974.

[13] N. T. H. Zhou Y., Gale W.F., “Modelling of transient liquid phase bonding,” *Int. Mater. Rev.*, vol. 40, no. 5, pp. 181–196, 1995.

[14] I. Tuah-Poku, M. Dollar, and T. Massalski, “A study of the transient liquid phase bonding process applied to a Ag/Cu/Ag sandwich joint,” *Metall. Trans. A*, vol. 19, no. March, pp. 675–686, 1988.

[15] deMarcos E. Schnell A, Stankowski A, “power for land, sea, air, Barcelona,” *Am. Soc. Mech. Eng.*, pp. 8–11, 2006.

[16] H. G. Jacobson D.M., *Principles of Brazing*. 2005.

[17] W. F. Gale and E. R. Wallach, "Microstructural development in transient liquid-phase bonding," *Metall. Trans. A*, vol. 22, no. 10, pp. 2451–2457, 1991.

[18] J. Ramirez and S. Liu, "Diffusion brazing in the nickel-boron system," *Weld. Journal-New York-*, no. October, pp. 365–376, 1992.

[19] K. C. Nakao Y., Nishimoto K., Shinozaki K., "Analysis of isothermal solidification process on transient liquid insert metal diffusion bonding," *Int. Inst. Weld.*, no. Document no. IA-334-86-OE, UK, 1986.

[20] Y. Zhou, "Analytical modeling of isothermal solidification during transient liquid phase (TLP) bonding," pp. 841–844, 2001.

[21] J. Crank, *The Mathematics of Diffusion*, Second Edi. 1975.

[22] T. C. Illingworth and I. O. Golosnoy, "Numerical solutions of diffusion-controlled moving boundary problems which conserve solute," *J. Comput. Phys.*, vol. 209, no. 1, pp. 207–225, 2005.

[23] J. Crank, *Free and moving boundary problems.* 1987.

[24] H. G. Landau, "Heat conduction in a melting solid," *Q. Appl. Math.*, vol. 8, pp. 81–94, 1950.

[25] W. Kass and M. O'Keeffe, "Numerical solution of Fick's equation with concentration-dependent diffusion coefficients," *J. Appl. Phys.*, vol. 37, no. 6, pp. 2377–2379, 1966.

[26] M. Ghezzo, "Diffusion from a Thin Layer into a Semi-Infinite Medium with Concentration Dependent Diffusion Coefficient. Part II," vol. 120, no. 8, pp. 1123–1127, 1973.

[27] C. Wagner, "Diffusion of lead chloride dissolved in solid silver chloride," *J. Chem. Phys.*, vol. 18, no. 9, pp. 1227–1230, 1950.

[28] R. Asthana, "An Analysis for Moving Boundary Diffusion Controlled Growth in a Finite Domain with a Concentration-Dependent Diffusion Coefficient," *J. Colloid Interface Sci.*, pp. 146–151, 1993.

[29] F. D. and G. S. C. R. Houska, "Time-Dependent Diffusion Coefficients Obtained From Diffused Films: The Cu-Ni System," *Thin Solid Films*, vol. 44, pp. 217–231, 1977.

[30] M. M. Abdelfatah and O. A. Ojo, "On the extension of processing time with increase in temperature during transient-liquid phase bonding," *Metall. Mater. Trans. A Phys. Metall. Mater. Sci.*, vol. 40, no. 2, pp. 377–385, 2009.

[31] O. A. Ojo and M. M. Abdelfatah, "On deviation from parabolic behaviour during transient liquid phase bonding," *Mater. Sci. Technol.*, vol. 24, no. 6, pp. 739–743, 2008.

[32] H. Liu, K. Wang, K. E. Aasmundtveit, and N. Hoivik, "Intermetallic compound formation mechanisms for

Cu-Sn solid-liquid interdiffusion bonding," *J. Electron. Mater.*, vol. 41, no. 9, pp. 2453–2462, 2012.

[33] C. W. Sinclair, G. R. Purdy, and J. E. Morral, "Transient liquid-phase bonding in two-phase ternary systems," *Metall. Mater. Trans. A*, vol. 31, no. 4, pp. 1187–1192, 2000.

[34] K. Bai, F. L. Ng, T. L. Tan, T. Li, and D. Pan, "Understanding non-parabolic solidification kinetics in Ni-based alloys during TLP bonding via thermo-kinetic modelling," *J. Alloys Compd.*, vol. 699, pp. 1084–1094, 2017.

[35] T. Takenaka, M. Kajihara, N. Kurokawa, and K. Sakamoto, "Reactive diffusion between Ag-Au alloys and Sn at solid-state temperatures," *Mater. Sci. Eng. A*, vol. 427, no. 1–2, pp. 210–222, 2006.

[36] D. E. Michael, "Analyses of Isothermal Solidification Kinetics during Transient Liquid Phase Bonding of Silver with Aluminium and Copper Filler Metals," University of Manitoba, 2018.

[37] S. Matsumoto, Y. Ishikawa, Y. Shirai, S. Sekine, and T. Niimi, "Concentration Dependence of the Diffusion Coefficient of Boron in Silicon," *Jpn. J. Appl. Phys.*, vol. 19, no. 1, p. 217, 1980.

[38] Z. Wang, L. Fang, I. Cotton, and R. Freer, "Ni – Cu interdiffusion and its implication for ageing in Ni-coated Cu conductors," *Mater. Sci. Eng. B*, vol. 198, pp. 86–94, 2015.

[39] Y.-H. Hwang, C.-F. Horng, S.-J. Lin, K.-S. Liu, and M.-T. Jahn, "Interface study for stainless steel fibre-reinforced aluminium matrix composite," *J. Mater. Sci.*, vol. 32, pp. 719–725, 1997.

[40] S. K. Mitra, S. K. Roy, and S. K. Bose, "Improvement of nonisothermal oxidation behavior of fe and fe-cr alloys by superficially applied reactive oxide coatings," *Oxid. Met.*, vol. 34, no. 1–2, pp. 101–121, 1990.

[41] D. K. O. J. Anderson, "Nonlinear Two-Step Diffusion in Semiconductors," *J. Electochemincal Soc.*, vol. 131, no. 11, pp. 2675–2679, 1984.